

REPORT DOCUMENTATION PAGE		READ INSTRUCTIONS BEFORE COMPLETING FORM
1. REPORT NUMBER	2. GOVT ACCESSION NO.	3. RECIPIENT'S CATALOG NUMBER
4. TITLE (and Subtitle) ACOUSTIC RADIATION FROM DOUBLE HULLS CONTAINING AN INNER FLUID		5. TYPE OF REPORT & PERIOD COVERED Technical Report No.29
		6. PERFORMING ORG. REPORT NUMBER
7. AUTHOR(s) J.M. Klosner and R. Vasudevan		8. CONTRACT OR GRANT NUMBER(s) N00014-78-C-0820
9. PERFORMING ORGANIZATION NAME AND ADDRESS Weidlinger Associates 333 Seventh Avenue New York, New York 10001		10. PROGRAM ELEMENT, PROJECT, TASK AREA & WORK UNIT NUMBERS 61153N 44023-03 064464
11. CONTROLLING OFFICE NAME AND ADDRESS Office of Naval Research Arlington, Virginia 22217		12. REPORT DATE January 1985
		13. NUMBER OF PAGES 63
14. MONITORING AGENCY NAME & ADDRESS (if different from Controlling Office)		15. SECURITY CLASS. (of this report)
		15a. DECLASSIFICATION/DOWNGRADING SCHEDULE
16. DISTRIBUTION STATEMENT (of this Report) Approved for Public Release; Distribution Unlimited		
17. DISTRIBUTION STATEMENT (of the abstract entered in Block 20, if different from Report)		
18. SUPPLEMENTARY NOTES		
19. KEY WORDS (Continue on reverse side if necessary and identify by block number) Acoustic Radiation Reinforced Cylindrical Shells Inner Fluid Hemispherical End Caps Concentric Shell Structure		
20. ABSTRACT (Continue on reverse side if necessary and identify by block number) The acoustic radiation characteristics of a fluid filled concentric shell structure are investigated by making use of the simple source surface integral method. The fluid field is described in terms of surface expansion functions, while the in vacuo structural modes, obtained by using the BOSOR4 structural program, are used as a basis for the shell motions. The structural code can be applied to branched shells of revolution, thereby obviating the need to introduce structural coupling of the two shells in a manner which is external to the main code.		

WEIDLINGER ASSOCIATES, CONSULTING ENGINEERS

333 SEVENTH AVENUE

NEW YORK, NEW YORK 10001

and

POLYTECHNIC INSTITUTE OF NEW YORK

BROOKLYN, NEW YORK 11201

ACOUSTIC RADIATION FROM CONCENTRIC SHELLS

CONTAINING AN INNER FLUID

By

J.M. Klosner and R. Vasudevan

OFFICE OF NAVAL RESEARCH

CONTRACT NO. N00014-78-C-0820

TECHNICAL REPORT NO. 29

(POLY M/AE REPORT 85-1)

Approved for Public Release; Distribution Unlimited

JANUARY 1985

WEIDLINGER ASSOCIATES, CONSULTING ENGINEERS
333 SEVENTH AVENUE
NEW YORK, NEW YORK 10001

and

POLYTECHNIC INSTITUTE OF NEW YORK
BROOKLYN, NEW YORK 11201

ACOUSTIC RADIATION FROM CONCENTRIC SHELLS

CONTAINING AN INNER FLUID

By

J.M. Klosner and R. Vasudevan

OFFICE OF NAVAL RESEARCH
CONTRACT NO. N00014-78-C-0820

TECHNICAL REPORT NO. 29
(POLY M/AE REPORT 85-1)

Approved for Public Release; Distribution Unlimited

JANUARY 1985

ABSTRACT

The acoustic radiation characteristics of a fluid filled concentric shell structure are investigated by making use of the simple source surface integral method. The fluid field is described in terms of surface expansion functions, while the in vacuo structural modes, obtained by using the BOSOR4 structural program, are used as a basis for the shell motions. The structural code can be applied to branched shells of revolution, thereby obviating the need to introduce structural coupling of the two shells in a manner which is external to the main code.

For illustrative purposes three types of internal harmonic excitations have been considered: (1) an axisymmetric unit pressure acting on the central region, (2) a unit line load acting on the central region, and (3) concentrated axial loads acting at the poles of the spherical closures. The far field fluid pressures have been obtained for a wide range of frequencies for both the single shell and for the double shell with and without inner fluid.

Because of numerical difficulties encountered when applying the integral methods to internal fluid problems, some simple approximations to the internal fluid problem were considered. The results obtained compare quite favorably with those of the exact solution over a wide range of frequencies.

TABLE OF CONTENTS

	<u>Page</u>
LIST OF SYMBOLS.....	i
I INTRODUCTION.....	1
II THEORY.....	4
1. Fluid Field.....	4
2. Surface Expansion Functions, Impedance Functions.....	7
3. Structural - Fluid Interaction.....	8
III APPLICATION TO THE DOUBLE SHELL.....	12
IV APPROXIMATE SOLUTIONS.....	17
1. Exact Solution.....	17
2. First-Order Approximation - Series Expansion.....	19
3. One Dimensional Approximation - Pipe Flow.....	23
V NUMERICAL CALCULATIONS AND RESULTS.....	26
REFERENCES.....	31
FIGURES.....	32

LIST OF SYMBOLS

a (b)	radius of inner (outer) shell
A_1 (A_2)	surface area of inner (outer) shell
c	acoustic velocity in fluid
d	distance between field and source points
D_{kj}	pressure influence coefficient associated with k th field point and j th source point
D_{kj}, n_k	velocity influence coefficient associated with k th field point and j th source point
G	free space Green's function
G_n	n th circumferential component of Green's function
h	distance between inner and outer shells
k	wave number
K	generalized stiffness of the structure
ℓ	length of cylindrical region
m, n	axial and circumferential mode numbers, respectively
M	generalized mass of the structure
n_p	normal to surface at location P
p	fluid pressure
q	generalized coordinate
\hat{q}	generalized coordinate associated with surface expansion function
Q	generalized force
\hat{Q}	generalized force associated with surface expansion function
r, θ , x	radial, circumferential and axial coordinates, respectively
R	mean radius ($R = \frac{a + b}{2}$)
s	meridional arc length of surface of revolution

S	source strength distribution function
U_m, V_m, W_m	axial, circumferential and normal components of m th structural mode
w	normal displacement component of shell
Z^j	impedance function associated with j th surface expansion function
z	radial coordinate measured from mean radius R
∇	Laplacian operator
ρ	fluid density
ϕ	velocity potential
ψ_k	k th surface expansion function
ω	frequency of excitation
ω_m	in-vacuo frequency of m th structural mode

I. INTRODUCTION

A vast amount of literature exists concerned with the problem of predicting sound radiation from submerged structures executing induced harmonic vibrations.

Except for some special geometries, for which analytical solutions can be achieved by the standard technique of separation of variables, the great majority of investigations have been carried out by using integral equation methods. Although some solutions have been obtained by applying the finite element methods these methods do not compare favorably with the simplicity and economy resulting from the use of the integral methods, especially so, because the problems of interest are generally those for which the fluid field is of infinite domain. The form of the integral equation method most often used to solve the radiation problem is referred to as the "simple source method". Here one assumes that the acoustic field potential is expressed in terms of a layer of monopole sources distributed over the radiating surface.

Upon invoking the compatibility relationship for the normal velocities at the interface, one obtains an integral equation for the unknown source density function. Once the density function is determined, one can compute the pressures and velocities throughout the fluid.

It should be noted that the use of the integral equation methods does present difficulties at and in the neighborhood of the characteristic frequencies associated with the interior Dirichlet problem. However, it has been pointed out by Piaczyk and Klosner [1] that the internal resonance problem which is

indeed present in the transducer type problem; i.e., when the velocity of the radiating surface is specified, does not occur in the structural radiation problem if the coupled equations are solved in the proper order.

In almost all of the investigations of structural radiation the fluid is in contact with only one side of the radiating surface. There is, however, a paucity of literature concerned with radiation from structures having internal and external wetted surfaces which interact with one another. One such investigation, carried out by Cambridge Acoustical Associates considered the radiation from a structure consisting of two flat plates separated by longitudinal structural membranes, and filled with a fluid. One side of the composite structure was in contact with a semi-infinite fluid, while the other side was in vacuo. A preliminary investigation of a more realistic situation was conducted at the Polytechnic Institute of New York. They considered the acoustic radiation from a structure consisting of concentric spherically capped cylindrical shells separated by, and immersed in, an acoustic fluid. The internal shell was stiffened, and the two shells were connected both structurally and acoustically.

In the present investigation the problem of radiation from a concentric shell structure is reconsidered by using a more refined and efficient approach.

First, surface expansion functions are used to describe the fluid fields. The expediency of using expansion functions have been amply demonstrated for both shock [2] and radiation [3]

problems. Their use results in reduced core memory requirements, thereby allowing for a more detailed description of the fluid fields, which is so necessary in order to accurately describe, in particular, the axisymmetric response of the inner fluid.

Second, the in vacuo structural modes, which are used to describe the shell motions, are obtained by using the BOSOR 4 structural program. This highly efficient program uses a circumferential modal expansion, and can be applied to branched shells of revolution, thereby eliminating the need to introduce structural coupling of the two shells in a manner which is external to the main code.

II. THEORY

Consider the acoustic radiation characteristics of a shell submerged in an acoustic medium and subjected to a time-harmonic excitation.

The velocities at the fluid-structural interface are expressed by sets of orthogonal functions. For the fluid, harmonic surface expansion functions are used, while for the structure the in vacuo structural modes serve as an expansion basis.

In the following, we will describe and formulate the procedure.

II.1 Fluid Field

The Helmholtz wave equation for an inviscid fluid undergoing simple harmonic motion is

$$(\nabla^2 + k^2)\phi = 0 \quad (2-1)$$

where ϕ = fluid velocity potential; the wave number $k = \omega/c$; c =acoustic velocity.

The particle velocity is expressed as the gradient of ϕ

$$\bar{v} = -\nabla\phi \quad (2-2)$$

and the pressure

$$p = \rho \frac{\partial\phi}{\partial t} \quad (2-3)$$

The solution of Eq. (2-1) corresponding to a unit source, i.e, the free space Green's function representing a divergent spherical wave, can be written as

$$G = -\frac{e^{-ikd}}{4\pi d} \quad (2-4)$$

where d =distance from source point Q to field point P . (Fig. 1)

For convenience, the time factor $e^{i\omega t}$ is suppressed here and is omitted in what follows, unless clarity demands its inclusion.

By invoking the Helmholtz integral

$$\epsilon\phi(P) = \frac{1}{4\pi} \left[\iint_{\sigma} G \frac{\partial\phi}{\partial n} d\sigma - \iint_{\sigma} \phi \frac{\partial G}{\partial n} d\sigma \right] \quad (2-5)$$

where $\epsilon = 0$, for P not in V , $\epsilon = \frac{1}{2}$ for P on boundary σ , and $\epsilon = 1$, P in V , we can express the value of ϕ at a point P in the region V in terms of ϕ and its normal derivative $\partial\phi/\partial n$ at the fluid bounding surface σ . The first integral of Eq. (2-5) represents the contribution to the potential due to a distribution of simple sources on the bounding surface, while the second term represents that due to distributed doublets with axes normal to the surface.

We can, under certain conditions, express the value of the potential in the region in terms of simple sources only, or doublets only, distributed over the fluid boundary. Expressed in terms of simple sources, the potential*

$$\phi(P) = -\frac{1}{4\pi} \iint_{\sigma} \frac{S}{d} e^{-ikd} d\sigma \quad (2-6)$$

where S denotes the source strength distribution function. Note that when point $P = p$ lies on the surface the integrand is singular, and the normal derivative becomes

$$\frac{\partial\phi}{\partial n}(p) = \frac{1}{2} S(p) - PV \left[\frac{1}{4\pi} \iint_{\sigma} S \frac{\partial}{\partial n} \left(\frac{e^{-ikd}}{d} \right) d\sigma \right] \quad (2-7)$$

where $PV =$ principal value.

When considering surfaces of revolution, (Fig. 2), it is expedient to use a circumferential harmonic expansion, so that

*This expression is invalid when k corresponds to the internal Dirichlet or Neumann eigenvalue problems (See Ref. 4, pp. 499, also Ref 1)

$$S = \sum_n S_n \cos n\theta \quad (2-8)$$

$$\phi = \sum_n \phi_n \cos n\theta \quad (2-9)$$

where

$$\phi_n(P) = \int_0^s G_n(P,Q) S_n(Q) ds \quad (2-10)$$

and the pressure influence coefficient

$$G_n(P,Q) = -\frac{r(Q)}{4\pi} \int_0^{2\pi} \frac{e^{-ikd}}{d} \cos n\psi d\psi \quad (2-11)$$

s is the arc length measured along the generator; r(Q) = distance from axis to generator at source point Q. Eq. (2-7) is now written as

$$\frac{\partial \phi_n(P)}{\partial n} = \frac{1}{2} S(P) + PV \left[\int_0^s \frac{\partial}{\partial n_p} [G_n(p,Q)] S_n(Q) ds \right] \quad (2-12)$$

and the velocity influence coefficient,

$$\frac{\partial}{\partial n_p} [G_n(p,Q)] = -\frac{r(Q)}{4\pi} \int_0^{2\pi} \frac{\partial}{\partial n_p} \left(\frac{e^{-ikd}}{d} \right) \cos n\theta d\theta \quad (2-13)$$

Of course, if the field point P does not lie on the surface, then

$$\frac{\partial \phi_n}{\partial n}(P) = \int_0^s \frac{\partial}{\partial n_p} [G_n(P,Q)] S_n(Q) ds \quad (2-14)$$

Upon subdividing the surface into N bands along the generator, and assuming that the source strength is constant along the generator within each band, we obtain the discretized forms of Eqs. (2-10), (2-12) and (2-14)

$$\phi_n(k) = \sum_{j=1}^N D_{kj} S_n(j) \quad (2-15a)$$

$$\frac{\partial \phi_n}{\partial n_k}(k) = \sum_{j=1}^N D_{kj, n_k} S_n(j) \quad (2-15b)$$

where D_{kj} and D_{kj, n_k} are the pressure and velocity influence

coefficients associated with reference to a field point P in the kth band and reference to a source point Q in the jth band.

II.2 SURFACE EXPANSION FUNCTIONS - IMPEDANCE FUNCTIONS

Since we are concerned with surfaces of revolution, a circumferential modal expansion is used. The solution for each circumferential wave number is obtained and the final result obtained by superposition.

Thus for each circumferential mode, an orthogonal set of fluid surface expansion functions ψ_k is chosen for use as an expansion basis for the normal component of the surface displacement w,

$$w = \sum_{k=1}^K \hat{q}_k \psi_k e^{i\omega t} \quad (2-16)$$

It is to be understood that all of the above ψ_k 's have the same harmonic circumferential variation, and that they have been normalized with respect to the surface area A, so that

$$\int_{\sigma} \psi_j \psi_k d\sigma = A \delta_{jk} \quad (2-17)$$

The impedance function Zj is defined as the surface pressure field pj, due to the surface velocity $-i\omega\psi_j$, and is determined by equating the normal components of the fluid velocity at the surface to that associated with the function ψ_j

$$\frac{\partial \phi}{\partial n} = -i\omega \psi_j \quad (2-18)$$

By appealing to Eqs. (2-15), we can express the above and the corresponding impedance function in matrix form,

$$\{-i\omega\psi_j^P\} = [D_{pQ, n_p}] \{S_Q\} \quad (2-19a)$$

$$\{Z_p^j\} = i\omega\rho[D_{pQ}]\{S_Q\} \quad (2-19b)$$

The simultaneous solution of Eqs. (2-14) then yields the source and impedance vectors S_Q and Z^j which are due to the surface velocity distribution- $i\omega\psi_j$.

In turn, we represent Z^j in terms of the surface expansion functions, so that

$$Z^j = \sum_{k=1}^K \frac{\gamma_{kj}}{A} \psi_k \quad (2-20)$$

where
$$\gamma_{kj} = \iint_{\sigma} Z^j \psi_k d\sigma = \Pi(1+\delta_{on}) \int_0^S r(s) Z^j \psi_k ds \quad (2-21)$$

$$\delta_{on} = \begin{cases} 1, n=0 \\ 0, n \neq 0 \end{cases} \quad (2-22)$$

Observe that γ_{kj} is the generalized force associated with the ψ_k -displacement and the pressure field arising from ψ_j .

II.3 STRUCTURAL-FLUID INTERACTION

The normal component of the displacement of the shell can be expressed as

$$w = \sum_{m=1}^M q_m W_m \quad (2-23)$$

where W_m = the w -component of the m th in vacuo shell mode, and q_m = m th generalized coordinate. Again it should be emphasized that all of the above modes are associated with one particular circumferential wave number.

For harmonic time-dependent steady-state motion, the shell equation of motion becomes

$$M_m(\omega_m^2 - \omega^2)q_m = Q_m^E + Q_m \quad (2-24)$$

where ω_m = in vacuo frequency of the m^{th} mode, the m^{th} component of the generalized mass and force is, respectively,

$$M_m = \iint_{\sigma} \rho h (U_m^2 + V_m^2 + W_m^2) d\sigma \quad (2-25)$$

$$Q_m = - \iint_{\sigma} p \phi_m d\sigma \quad (2-26)$$

and Q_m^E = generalized force associated with the applied loads. U_m, V_m, W_m are the shell displacements along the generator and in the circumferential and normal directions, respectively.

At the shell-fluid interface, the normal shell velocity must be equal to the normal fluid particle velocity. Hence

$$i\omega w = i\omega \sum_{m=1}^M q_m W_m = i\omega \sum_{k=1}^K \hat{q}_k \psi_k \quad (2-27)$$

Making use of the orthogonality relationship, we have

$$\hat{q}_k = \sum_{m=1}^M \lambda_{km} q_m \quad (2-28)$$

where
$$\lambda_{km} = \frac{1}{A} \iint_{\sigma} W_m \psi_k d\sigma \quad (2-29)$$

Expressing the surface pressure in the form of series expansions in both the surface expansion functions and the in vacuo structural modes, we obtain the following

$$p = \sum_{m=1}^M \frac{Q_m}{\mu_m} W_m = - \sum_{k=1}^K \frac{\hat{Q}_k}{A} \psi_k \quad (2-30)$$

where the associated generalized forces

$$Q_m = - \iint_{\sigma} p W_m d\sigma \quad (2-31)$$

$$\hat{Q}_k = - \iint_{\sigma} p \psi_k d\sigma \quad (2-32)$$

are related as follows:

$$Q_m = \sum_{k=1}^K \frac{\hat{Q}_k}{A} \iint_{\sigma} W_m \psi_k d\sigma = \sum_{k=1}^K \lambda_{mk} \hat{Q}_k \quad (2-33)$$

Recall that p_j denotes the surface pressure due to the surface velocity ψ_j . Thus, upon observing Eq. (2-16), we note that the pressure due to the actual surface velocity can be written as

$$p = \sum_{j=1}^K \hat{q}_j z^j \quad (2-34)$$

Upon substituting Eq. (2-34) into Eq. (2-32), we obtain

$$\hat{Q}_k = - \sum_{j=1}^K \hat{q}_j \iint_{\sigma} z^j \psi_k d\sigma \quad (2-35)$$

which, upon substituting (2-21) and (2-28), becomes

$$\hat{Q}_k = - \sum_{j=1}^K \gamma_{kj} \hat{q}_j = - \sum_{j=1}^K \gamma_{kj} \sum_{m=1}^M \lambda_{jm} q_m \quad (2-36)$$

Combining Eqs. (2-33) and (2-36) then yields

$$Q_m = - \sum_{k=1}^K \sum_{j=1}^K \sum_{m=1}^M \lambda_{nk} \lambda_{jm} \gamma_{kj} q_m \quad (2-37)$$

The substitution of Eq. (2-37) into the equations of motion (2-24), leads to the following set of coupled simultaneous equations, expressed in matrix notation,

$$[K - \omega^2 M + L] \{q\} = \{Q^E\} \quad (2-38)$$

where

$$[K] = [\omega_m^2 M_m] \quad (2-39)$$

$$[\omega^2 M] = [\omega^2 M_m]$$

$$[L] = [\lambda_{km}]^T [\gamma_{kj}] [\lambda_{jm}]$$

The solution of the above equation yields the generalized coordinate vector q . By substituting q into Eq. (2-28) and then into Eq. (2-34), we obtain an expansion for the surface pressures at the i nodes (or bands) ($i = 1 \rightarrow I$)

$$\{p_i\} = [Z_{ij}][\lambda_{jm}]\{q_m\} \quad (2-40)$$

where $Z_{ij} = Z_{ij}$ = the value of the impedance function at the i th node associated with the ψ_j surface displacement.

The far-field pressure is then obtained by substituting the source strength vector S^j into the discretized form of Eq. (2-10) and thereupon substituting into Eq (2-3). Thus the far-field pressure at point P ,

$$p(P) = i\omega\rho\{G_i(P)\}^T [S_{ij}][\lambda_{jm}]\{q_m\} \quad (2-41)$$

where $G_i(P)$ = pressure influence coefficient vector, $[G_i(p) = G(P,i)]$

S_{ij} = element of source strength vector

$[S_{ij} = \Delta s_i S_i^j = \text{product of } i\text{th band width and value of } S^j \text{ at } i\text{th node}]$

III. APPLICATION TO THE DOUBLE HULL SHELL

We now consider the concentric capped cylindrical shell (Fig 3), and define a set of surface expansion functions for the inner and outer shells ψ_k^I and ψ_k^{II} , respectively. Following along the lines described in Section II, we have that

$$w^I = \sum_{m=1}^M q_m W_m^I = \sum_{k=1}^{K1} \hat{q}_k^I \psi_k^I \quad (3-1)$$

$$w^{II} = \sum_{m=1}^M q_m W_m^{II} = \sum_{k=1}^{K2} \hat{q}_k^{II} \psi_k^{II} \quad (3-2)$$

where the subscript I and II refers to the inner and outer shell, respectively, and all of the above functions have a common circumferential wave number n. W_m is the normal component of the mth in vacuo mode of the branched shell structure, and W_m^I and W_m^{II} refer to that part of W_m associated with the surfaces of the inner and outer shells, respectively. $K1$ and $K2$ are the number of expansion functions used for the inner and outer surfaces, respectively.

As in Section II, we have that

$$\hat{q}_k^I = \sum_{m=1}^M \lambda_{km}^I q_m \quad (3-3)$$

$$\hat{q}_k^{II} = \sum_{m=1}^M \lambda_{km}^{II} q_m \quad (3-4)$$

where
$$\lambda_{km}^I = \frac{1}{A_1} \iint_{\sigma_1} W_m^I \psi_k^I d\sigma \quad (3-5)$$

$$\lambda_{km}^{II} = \frac{1}{A_2} \iint_{\sigma_2} W_m^{II} \psi_k^{II} d\sigma \quad (3-6)$$

We define the impedance functions z_{k1}^j as the pressure at the kth surface due to the surface expansion ψ_j at the l-th shell surface. It is evaluated by following a procedure similar to that for a single shell*. For the inner fluid the discretized form of the compatibility equation (2-12) is applied to all wetted nodes of the inner fluid; for example, when the fluid velocity is $-i\omega\psi_j^I$ it is implied that $\frac{\partial\phi}{\partial n} \equiv 0$ at all nodal points lying on the outer shell. When considering the outer fluid, the impedance function is determined by using the procedure described for the single shell. Thus for the inner fluid the impedance functions associated with the displacement ψ_j^I along the inner shell are expressed as

$$z_{11}^j = \sum_{k=1}^{K1} \frac{\gamma_{kj}^{11}}{A_1} \psi_k^I \quad (3-7)$$

$$z_{21}^j = \sum_{k=1}^{K2} \frac{\gamma_{kj}^{21}}{A_2} \psi_k^{II} \quad (3-8)$$

*As a consequence of the fact that the normal direction is always assumed to be positive outward, the term $1/2 S(p)$ which appears in Eq. (2-7) is replaced by $-1/2 S(p)$ when considering the inner fluid in contact with the outer shell.

while those associated with the displacement distribution ψ_j^{II} of the outer shell are

$$z_{22}^j = \sum_{k=1}^{K2} \frac{\gamma_{kj}^{22}}{A_2} \psi_k^{II} \quad (3-9)$$

$$z_{12}^j = \sum_{k=1}^{K1} \frac{\gamma_{kj}^{12}}{A_1} \psi_k^I \quad (3-10)$$

where

$$\gamma_{kj}^{11} = \iint_{A_1} z_{11}^j \psi_k^I d\sigma \quad (3-11)$$

$$\gamma_{kj}^{21} = \iint_{A_2} z_{21}^j \psi_k^{II} d\sigma \quad (3-12)$$

and

$$\gamma_{kj}^{22} = \iint_{A_2} z_{22}^j \psi_k^{II} d\sigma \quad (3-13)$$

$$\gamma_{kj}^{12} = \iint_{A_1} z_{12}^j \psi_k^I d\sigma \quad (3-14)$$

The subscripts and superscripts 1 and 2 respectively denote the surfaces of the inner and outer shells which are in contact with the inner fluid.

Finally, for the outer fluid

$$z_{33}^j = \sum_{k=1}^{K2} \frac{\gamma_{kj}^{33}}{A_2} \psi_k^{II} \quad (3-15)$$

$$\gamma_{kj}^{33} = \iint_{A_2} z_{33}^j \psi_k^{II} d\sigma \quad (3-16)$$

One can readily show that the components of the generalized force associated with the interaction fluid pressures are

$$Q_n^{11} = -\sum_{k=1}^{K1} \sum_{j=1}^{K1} \sum_{m=1}^M \lambda_{nk}^I \gamma_{kj}^{11} \lambda_{jm}^I q_m \quad (3-17)$$

$$Q_n^{21} = \sum_{k=1}^{K2} \sum_{j=1}^{K1} \sum_{m=1}^M \lambda_{nk}^{II} \gamma_{kj}^{21} \lambda_{jm}^I q_m \quad (3-18)$$

$$Q_n^{22} = \sum_{k=1}^{K2} \sum_{j=1}^{K2} \sum_{m=1}^M \lambda_{nk}^{II} \gamma_{kj}^{22} \lambda_{jm}^{II} q_m \quad (3-19)$$

$$Q_n^{12} = -\sum_{k=1}^{K1} \sum_{j=1}^{K2} \sum_{m=1}^M \lambda_{nk}^I \gamma_{kj}^{12} \lambda_{jm}^{II} q_m \quad (3-20)$$

and

$$Q_n^{33} = -\sum_{k=1}^{K2} \sum_{j=1}^{K2} \sum_{m=1}^M \lambda_{nk}^{II} \gamma_{kj}^{33} \lambda_{jm}^{II} q_m \quad (3-21)$$

where the negative signs appear on the right hand sides of the expressions for $Q_n^{11}, Q_n^{12}, Q_n^{33}$ because positive pressures are in the opposite direction to positive radial displacements for these cases.

The shell equation for time-harmonic motion is

$$M_m (\omega_m^2 - \omega^2) q_m = Q_m^E + Q_m^{11} + Q_m^{21} + Q_m^{22} + Q_m^{12} + Q_m^{33} \quad (3-22)$$

$$[K - \omega^2 M - L] \{q\} = \{Q^E\} \quad (3-23)$$

where K and $\omega^2 M$ have been previously defined [Eq 2-39] and

here

$$\begin{aligned} L = & -[\lambda_{km}^I][\gamma_{kj}^{11}][\lambda_{jm}^I] + [\lambda_{km}^{II T}][\gamma_{kj}^{21}][\lambda_{jm}^I] \\ & + [\lambda_{km}^{II T}][\gamma_{kj}^{22}][\lambda_{jm}^{II}] - [\lambda_{km}^I T][\gamma_{kj}^{12}][\lambda_{jm}^{II}] - [\lambda_{km}^{II T}][\gamma_{kj}^{33}][\lambda_{jm}^{II}] \end{aligned} \quad (3-24)$$

Utilizing the q -matrix found from Eq. (3-23), we can determine the pressure at the surface nodes from the following expressions

$$\{p^I\} = [Z_{11}^j][\lambda_{jm}^I]\{q_m\} + [Z_{12}^j][\lambda_{jm}^{II}]\{q_m\} \quad (3-25)$$

and
$$\{p^{II}\} = [Z_{33}^j - Z_{22}^j] [\lambda_{jm}^{II}\{q_m\}] - [Z_{21}^j] [\lambda_{jm}^I\{q_m\}] \quad (3-26)$$

The far-field pressures are obtained by simply applying the form given by Eq. (2-41) to the outer fluid.

IV. APPROXIMATE SOLUTIONS

Serious numerical difficulties are encountered when applying the integral methods to solve radiation problems for an enclosed fluid. As a consequence, the number of nodes (or bands) required to obtain accurate results must be greatly increased over that which is required for the external fluid. In addition much greater detail has to be introduced when evaluating the fluid influence coefficient integrals. Because of this, a preliminary investigation of some simple approximations was undertaken.

Consider a fluid region within two concentric cylindrical surfaces and end closure rings as shown in Fig. 4. Let the normal displacement of the inner surface be of the form $\cos\left(\frac{m\pi x}{\ell}\right) \cos n\theta e^{i\omega t}$, and let the outer surface and the end closure rings be rigid. For this problem first the exact solution is obtained and then approximations of the fluid field are developed for the situation when the gap between the two cylinders is small.

IV.1 Exact Solution

The fluid field potential is represented by the wave equation

$$\frac{\partial^2 \phi}{\partial r^2} + \frac{1}{r} \frac{\partial \phi}{\partial r} + \frac{1}{r^2} \frac{\partial^2 \phi}{\partial \theta^2} + \frac{\partial^2 \phi}{\partial x^2} = \frac{1}{c^2} \frac{\partial^2 \phi}{\partial t^2} \quad (4-1)$$

where r, θ, x , are cylindrical coordinates. For the problem

described above, the boundary conditions are,

$$\frac{\partial \phi}{\partial r}(r=a) = -i\omega \cos\left(\frac{m\pi x}{\ell}\right) \cos n\theta e^{i\omega t} \quad (4-2)$$

$$\frac{\partial \phi}{\partial r}(r=b) = 0 \quad (4-3)$$

$$\frac{\partial \phi}{\partial x}(x=0, \ell) = 0 \quad (4-4)$$

The general solution of Eq. (4-1), satisfying the boundary condition in Eq. (4-4) is

$$\phi = \sum_{m=0}^{\infty} \sum_{n=0}^{\infty} [A_{mn} f_n(k_m r) + B_{mn} g_n(k_m r)] \cos n\theta \cos\left(\frac{m\pi x}{\ell}\right) e^{i\omega t} \quad (4-5)$$

where

$$k_m = \sqrt{\frac{\omega^2}{c^2} - \frac{m^2 \pi^2}{\ell^2}} \quad \text{for } \frac{\omega^2}{c^2} \geq \frac{m^2 \pi^2}{\ell^2} \quad (4-6a)$$

and f_n, g_n are Bessel functions of the 1st and 2nd kind of order n ,

$$\text{or } k_m = \sqrt{\frac{m^2 \pi^2}{\ell^2} - \frac{\omega^2}{c^2}} \quad \text{for } \frac{\omega^2}{c^2} < \frac{m^2 \pi^2}{\ell^2} \quad (4-6b)$$

and f_n, g_n are the modified Bessel functions.

The constants A_{mn} and B_{mn} are determined from Eqs. (4-2) and (4-3), and thus Eq. (4-5) can be written as

$$\phi = \sum_{m=0}^{\infty} \sum_{n=0}^{\infty} \frac{i\omega}{k_m} \frac{[f'_n(k_m b)g_n(k_m r) - g'_n(k_m b)f_n(k_m r)]}{[f'_n(k_m a)g'_n(k_m b) - f'_n(k_m b)g'_n(k_m a)]} \cos n\theta \cos\left(\frac{m\pi x}{\ell}\right) e^{i\omega t} \quad (4-7)$$

where $f'_n(\) = \frac{\partial f_n}{\partial(\)}$

The velocity and pressure fields are then obtained by substituting into Eqs. (2-2) and (2-3)

IV.2 FIRST-ORDER APPROXIMATION - Series Expansion

For the region shown in Fig. 4, we express the fluid potential in terms of a three-term series expansion through the thickness,

$$\phi = f_0(x, \theta, t) + z f_1(x, \theta, t) + z^2 f_2(x, \theta, t) \quad (4-8)$$

where $z = r - R \left(-\frac{h}{2} \leq z \leq \frac{h}{2} \right)$ (4-9)

the mean radius $R = \frac{a+b}{2}$ (4-10)

and the gap $h = b - a$ (4-11)

The fluid equations of motion can be expressed in terms of Hamilton's variational principle,

$$\delta \left[\int_{t_1}^{t_2} L dt + \int_{t_1}^{t_2} W dt \right] = 0 \quad (4-12)$$

where the Lagrangian

$$L = \frac{1}{2} \iiint \left\{ \rho \left[\left(\frac{\partial \phi}{\partial r} \right)^2 + \left(\frac{\partial \phi}{r \partial \theta} \right)^2 + \left(\frac{\partial \phi}{\partial x} \right)^2 \right] - \frac{\rho}{c} \left(\frac{\partial \phi}{\partial t} \right)^2 \right\} dV \quad (4-13)$$

and the work done by the pressure at the boundaries

$$W = \pm \frac{1}{2} \iint_{\sigma} \rho v_n \frac{\partial \phi}{\partial t} d\sigma \quad (4-14)$$

The (+) sign refers to the surfaces $r=a$ and $x=0$, and the (-) sign

refers to the surfaces $r=b$ and $x=l$, and v_n = normal surface velocity (positive in positive r and x directions).

The variational equation (4-12) can thus be written as

$$\rho \int_{t_1}^{t_2} \left[\left\{ \frac{\partial \phi}{\partial r} \delta \frac{\partial \phi}{\partial r} + \frac{1}{r^2} \frac{\partial \phi}{\partial \theta} \delta \frac{\partial \phi}{\partial \theta} + \frac{\partial \phi}{\partial x} \delta \frac{\partial \phi}{\partial x} - \frac{1}{c^2} \frac{\partial \phi}{\partial t} \delta \frac{\partial \phi}{\partial t} \right\} r d\theta dr dx \right] dt + \rho \int_{t_1}^{t_2} \left[\iint_{\sigma} v_n \delta \frac{\partial \phi}{\partial t} d\sigma \right] dt \quad (4-15)$$

which upon integrating by parts and enforcing the condition that the variation vanishes at the end points, becomes

$$\begin{aligned} & -\rho \int_{t_1}^{t_2} \left[\iiint \left\{ \frac{1}{r} \frac{\partial}{\partial r} \left(r \frac{\partial \phi}{\partial r} \right) + \frac{1}{r^2} \frac{\partial^2 \phi}{\partial \theta^2} + \frac{\partial^2 \phi}{\partial x^2} - \frac{1}{c^2} \frac{\partial^2 \phi}{\partial t^2} \right\} \delta \phi r d\theta dr dx \right] dt \\ & + \rho \int_{t_1}^{t_2} \left[\iiint \left(\frac{\partial \phi}{\partial r} + v_n \right) \delta \phi \Big|_{z=-h/2}^{z=h/2} r d\theta dx + \iint \left(\frac{\partial \phi}{\partial x} + v_n \right) \delta \phi \Big|_{x=0}^{x=l} r d\theta dr \right] dt = 0 \end{aligned} \quad (4-16)$$

The evanescence of the above surface integral simply leads to the interface boundary conditions

$$\frac{\partial \phi}{\partial r} = -v_n \text{ at } z = \pm h/2$$

and

$$\frac{\partial \phi}{\partial x} = -v_n \text{ at } x=0, l$$

(4-17)

If we introduce Eq. (4-8) into Eq. (4-17), then

$$-v_n(b) = \frac{\partial \phi}{\partial r}(b) = \frac{\partial \phi}{\partial z}(h/2) = f_1 + hf_2$$

$$-v_n(a) = \frac{\partial \phi}{\partial r}(a) = \frac{\partial \phi}{\partial z}(-h/2) = f_1 - hf_2$$

(4-18)

and thus

$$f_1 = -\frac{1}{2} [v_n(b) + v_n(a)]$$

$$f_2 = -\frac{1}{2h} [v_n(b) - v_n(a)]$$

(4-19)

Since f_1 and f_2 are expressed in terms of the surface displacements,

$$\delta\phi = \delta f_0 \quad (4-20)$$

It should be noted that this procedure can easily be generalized to include a higher - order expansion function.

Upon utilizing the approximation

$$\frac{1}{R+Z} \approx \frac{1}{R} - \frac{Z}{R^2} \quad (4-21)$$

and integrating through the thickness, Eq. (4-16) takes the following form

$$\int_{t_1}^{t_2} [\int \{ 2Rh f_2 + h f_1 + \frac{h}{R} f_{o,\theta\theta} - \frac{h^3}{12R} 2 f_{1,\theta\theta} + \frac{h^3}{12R} f_{2,\theta\theta} + Rh f_{o,xx} + \frac{h^3}{12} f_{1,xx} + \frac{Rh^3}{12} f_{2,xx} - \frac{1}{c^2} (Rh f_{o,tt} + \frac{h^3}{12} f_{1,tt} + \frac{Rh^3}{12} f_{2,tt}) \} \delta f_0 r d\theta dx] dt = 0 \quad (4-22)$$

Setting the above integrand equal to zero, we obtain the differential equation for f_0 ,

$$f_{o,xx} + \frac{1}{R^2} f_{o,\theta\theta} - \frac{1}{c^2} f_{o,tt} = -2f_2 - \frac{1}{R} f_1 - \frac{h^2}{12R} [-\frac{1}{R^2} f_{1,\theta\theta} + \frac{1}{R} f_{2,\theta\theta} + f_{1,xx} + R f_{2,xx} - \frac{1}{c^2} f_{1,tt} - \frac{R}{c^2} f_{2,tt}] \quad (4-23)$$

Since $h/R \ll 1$, the terms appearing in the bracket are neglected and the final equation is

$$f_{o,xx} + \frac{1}{R^2} f_{o,\theta\theta} - \frac{1}{c^2} f_{o,tt} = -2f_2 - \frac{1}{R} f_1 \quad (4-24)$$

Letting

$$f_i = f_i(x) \cos n\theta e^{i\omega t} \quad (4-25)$$

we have
$$f_{o,xx} + \left(\frac{\omega^2}{c^2} - \frac{n^2}{R^2}\right) f_o = -\left(2f_2 + \frac{1}{R} f_1\right) \quad (4-26)$$

We can reformulate the problem in terms of the pressure, so that

$$P = (p_o + z p_1 + z^2 p_2) \cos n\theta e^{i\omega t} \quad (4-27)$$

and the equivalent of Eqs. (4-26) and (4-19) are

$$p_{o,xx} + \left(\frac{\omega^2}{c^2} - \frac{n^2}{R^2}\right) p_o = -(2p_2 + \frac{1}{R} p_1) \quad (4-28)$$

and

$$p_1 = -i\rho\omega \left[\frac{v_n(b) + v_n(a)}{2} \right]$$

$$p_2 = -i\rho\omega \left[\frac{v_n(b) - v_n(a)}{2h} \right] \quad (4-29)$$

For the problem described in the beginning of this section (Fig. 4), $v_n(a) = i\omega \cos \frac{m\pi x}{\ell} \cos n\theta e^{i\omega t}$

$$v_n(b) = 0 \quad (4-30)$$

and since the end closure rings are assumed to be rigid

$$\frac{\partial \phi}{\partial x} = 0 \text{ at } x = 0, \ell \quad (4-31)$$

or alternatively

$$\frac{\partial p}{\partial x} = 0 \text{ at } x = 0, \ell \quad (4-32)$$

By substituting Eqs. (4-30) into (4-29), we note that P_1 and P_2 identically satisfy this last condition, and it is thus necessary that

$$\frac{\partial P}{\partial x} = 0 \text{ at } x = 0, \ell \quad (4-33)$$

Applying these end conditions to the solution of Eq. (4-28), results in the following

$$p_o = \left\{ \frac{2a\rho\omega^2}{b^2 - a^2} \left/ \left[\frac{\omega^2}{c^2} - \frac{n^2}{R^2} - \left(\frac{m\pi}{\ell}\right)^2 \right] \right. \right\} \cos \frac{m\pi x}{\ell} \quad (4-34)$$

The pressures can thereupon be expressed as

$$p = \rho \omega^2 \left\{ \frac{2a}{[b^2 - a^2] \left[\frac{\omega^2}{c^2} - \frac{n^2}{R^2} - \left(\frac{m\pi}{\ell} \right)^2 \right]} + \frac{1}{2} z - \frac{z^2}{2(b-a)} \right\} \cos \frac{m\pi x}{\ell} \cos n\theta e^{i\omega t} \quad (4-35)$$

IV. 3 ONE-DIMENSIONAL APPROXIMATION - "PIPE FLOW"

The linearized form of the continuity and momentum equations for inviscid, compressible flow are:

$$\frac{\partial \rho}{\partial t} + \rho \nabla \cdot \bar{v} = 0 \quad (4-36)$$

$$-\frac{1}{\rho} \nabla p = \frac{\partial \bar{v}}{\partial t} \quad (4-37)$$

Since the acoustic velocity

$$c = \left(\frac{\partial p}{\partial \rho} \right)^{1/2} \quad (4-38)$$

we can rewrite the continuity equation as

$$\frac{1}{c^2} \frac{\partial p}{\partial t} + \rho \nabla \cdot \bar{v} = 0. \quad (4-39)$$

where in cylindrical coordinates

$$\nabla \cdot \bar{v} = \frac{1}{r} \frac{\partial}{\partial r} (ru_r) + \frac{1}{r} \frac{\partial u_\theta}{\partial \theta} + \frac{\partial u_z}{\partial z} \quad (4-40)$$

The one-dimensional axi-symmetric or "pipe-flow" approximation is obtained by satisfying the continuity and momentum equations on an average by integrating them through the thickness. The resulting one-dimensional forms of the continuity and momentum equations are

$$\frac{1}{c^2} \frac{\partial p^*}{\partial t} + \rho \frac{2[b u_r(b) - a u_r(a)]}{(b^2 - a^2)} + \frac{\partial u_x^*}{\partial x} = 0 \quad (4-41)$$

and
$$\frac{1}{\rho} \frac{\partial p^*}{\partial x} = \frac{\partial u_x^*}{\partial t} \quad (4-42)$$

where
$$p^* = \frac{2 \int_a^b p r dr}{(b^2 - a^2)} \quad (4-43)$$

$$u_x^* = \frac{2 \int_a^b u_x r dr}{(b^2 - a^2)} \quad (4-44)$$

Upon taking the temporal derivative of Eq. (4-41) and the spatial derivative of Eq (4-42), and combining them, we are led to the "pipe-flow" equation

$$\frac{1}{c^2} \frac{\partial^2 p^*}{\partial t^2} = \frac{\partial^2 p^*}{\partial x^2} - \rho \left\{ \frac{2[b \frac{\partial u_r}{\partial t}(b) - a \frac{\partial u_r}{\partial t}(a)]}{(b^2 - a^2)} \right\} \quad (4-45)$$

For the axisymmetric problem presented in the previous section, (n=0),

$$u_r(a) = i\omega \cos \frac{m\pi x}{\ell} e^{i\omega t}$$

$$u_r(b) = 0 \quad (4-46)$$

and the velocities at the end closures vanish,

$$u_x^*(0) = u_x^*(\ell) = 0 \quad (4-47)$$

Thus, the boundary-value problem reduces to

$$\frac{\partial^2 p^*}{\partial x^2} + \frac{\omega^2}{c^2} p^* = \frac{2a\omega^2 \rho}{(b^2 - a^2)} \cos \frac{m\pi x}{\ell} e^{i\omega t}$$

and

$$\frac{\partial p^*}{\partial x}(0) = \frac{\partial p^*}{\partial x}(\ell) = 0 \quad (4-48)$$

and its solution is

$$p^* = \frac{2a\omega^2 \rho}{(b^2 - a^2) \left[\frac{\omega^2}{c^2} - \left(\frac{m\pi}{\ell} \right)^2 \right]} \cos \frac{m\pi x}{\ell} e^{i\omega t} \quad (4-49)$$

V. Numerical Calculations and Results

The geometry of the capped concentric cylindrical shell used in the calculations is shown in Figure 3. For illustrative purposes three types of internal harmonic excitations have been considered: (1) an axisymmetric unit pressure acting on the central region over a length of 22.5", (2) a unit line load acting along the central region, and (3) concentrated axial loads acting at the poles of the spherical closures.

The fluid pressure field has been obtained for nondimensional frequencies ranging from $ka = 0.18$ to 3.52 for the single shell and for the shell with and without inner fluid.

Because of the longitudinal symmetry of the loading functions, only longitudinally symmetrical structural modes and surface expansion functions were used. Calculations were carried out by using a total of 80 structural modes and 35 surface expansion functions for each of the first four circumferential modes (i.e. for $n=0,1,2,3$). The impedance functions for each of the surface expansion functions were obtained by subdividing each of the wetted surfaces into 180 discrete bands (15 bands for each sphere, and the remaining 150 bands located on the cylinder), so that the band widths were approximately 1.5 in.

The pressure and velocity influence coefficients were calculated by using surface integrals for the self-influence coefficients, and line integrals elsewhere. However for the axisymmetric mode, $n=0$, all influence coefficients pertaining to the inner fluid were evaluated by means of surface integrals. This was necessary because of the extreme sensitivity of the axisymmetric response of the inner fluid to numerical inaccuracies, especially at low frequencies.

All calculations were performed on the CYBER 176. The execution time required to obtain 80 structural modes for a particular circumferential mode number was approximately 30 secs for the single shell case, and 90 secs for the double shell. For the single shell about 3 minutes of execution time was required to calculate the influence coefficients and impedance functions associated with all of the surface expansion functions, and an additional 20 sec were required to calculate the structural responses and the far-field pressures. These were increased to 20 minutes and 40 secs, respectively for the case of the double shell.

The physical constants used for all calculations are:

FLUID

$$\text{(Density)} \rho = 9.45216 \times 10^{-5} \text{ lb-sec}^2/\text{in}^4$$

$$\text{(Acoustic Velocity)} c = 60,000 \text{ in/sec}$$

STEEL SHELL

$$\text{(Density)} \rho = 73.3 \times 10^{-5} \text{ lb-sec}^2/\text{in}^4$$

$$\text{(Acoustic Velocity)} c = 202,284 \text{ in/sec}$$

Results for the far field pressure at points located 32 radius ($R = 32a_i$) from the geometric center of the structure are shown in Figures (5-21)

The radiated pressure field for the axisymmetric loading of the central compartment is shown in Figs (5-10). The results indicate that at the lower frequencies the coupling affected by the inner fluid has little effect upon the radiated pressure. However, no general trend can be observed as to the efficacy of using a particular shell construction to reduce the far field radiation. Indeed, one can note

that the relative radiation characteristics of the shell configurations vary with frequency. Of course, it is well known that the relationship between the forcing frequency and the in-fluid resonant frequency of the structure is the primary factor in determining the magnitude of the far field pressures.

Figs (11-15) show the results for the line load acting on the central compartment, while Figs. (16-21) present the results for the end cap loadings. For these cases, as for the previous case, no general trend is observed.

Because of numerical difficulties encountered when applying the integral methods to problems in which internal fluids are present, an investigation of some simple approximations to the internal fluid problem was undertaken. As a vehicle for this preliminary investigation, the problem of two concentric circular cylindrical shells separated by a small gap, which is filled with an acoustic fluid, was considered (Fig. 4). The outer cylinder and the end closure rings were assumed to be rigid, and the normal displacement of the inner cylinder was assumed to vary cosinusoidally in both the circumferential direction and along its generator.

Two approximations were considered - a first order approximation, in which the fluid potential is expressed in terms of a three-term series expansion through the thickness, and a simple one-dimensional or "pipe flow" approximation. A comparison of the results obtained from these approximations to those determined analytically from the exact formulation is given in Fig (22 - 32). It should be noted that the very large pressures obtained are simply due to the fact that a unit displacement amplitude of the inner

cylinder was used.

For the axisymmetric case ($n=0$), Figs (22-26), the first-order approximation yields excellent results over a wide frequency band. The lowest frequency for which the approximation is valid varies from $ka = 0.088$ at the axial wave number, $m = 0$ to $ka = 1.58$ at $m=8$. At the highest frequency for which calculations have been performed ($ka = 4.40$) the maximum error is about 3%. It should be noted that the one-dimensional approximation yields good results over a more restricted frequency range, i.e., the error is within 2% for $ka = 0.88$ to 1.76 for $m=0$ and for $ka = 1.67$ to 2.11 for $m=8$.

For the asymmetric cases the one-dimensional approximations is invalid. However the first-order approximation yields results that are within 2% in error over the range of $ka = 0.088 - 4.40$ for $n=1, m=0$ and over the range of $ka = 1.67 - 4.40$ for $n=1, m=8$. Similar results are obtained for the $n=2$ modes.

It should be noted that the first-order approximation yields excellent results over the frequency range where the exact solution is expressed in terms of the ordinary Bessel function, i.e. when $\omega^2/c^2 \geq m^2\pi^2/\ell^2$. When $\omega^2/c^2 < m^2\pi^2/\ell^2$ these functions are replaced by the modified Bessel functions, and the three-term series approximation no longer yields meaningful results, pointing out that a higher-order series approximation is required.

Thus this preliminary investigation of the first-order approximations has illustrated that such a series expansion through the thickness does lead to a significant reduction of the effort required to determine the far field radiation characteristics

for structures which contain an internal fluid. To accommodate a larger frequency range, and consider more complex geometries for which an internal fluid is present, a higher-order series expansion is required.

REFERENCES

1. Piaszczyk, C.M. and Klosner, J.M., "Acoustic Radiation From Vibrating Surfaces at Characteristic Frequencies", J. Acoust. Soc. Amer., Vol. 75, No. 2, February 1984, pp. 363-375.
2. Ranlet, D., DiMaggio, F.L., Bleich, H.H. and Baron, M.L., "Elastic Response of Submerged Shells with Internally Attached Structures to Shock Loading", Computers & Structures, Vol. 7, pp. 355-364.
3. Sandman, B.E., "Spatial Fourier Decomposition: Analysis of Fluid-Loaded Structural Vibration", Naval Underwater Systems Center, Newport Laboratory TM No. 79-2039, January 25, 1979.
4. Lamb, H., Hydrodynamics, Dover, New York, 1945.

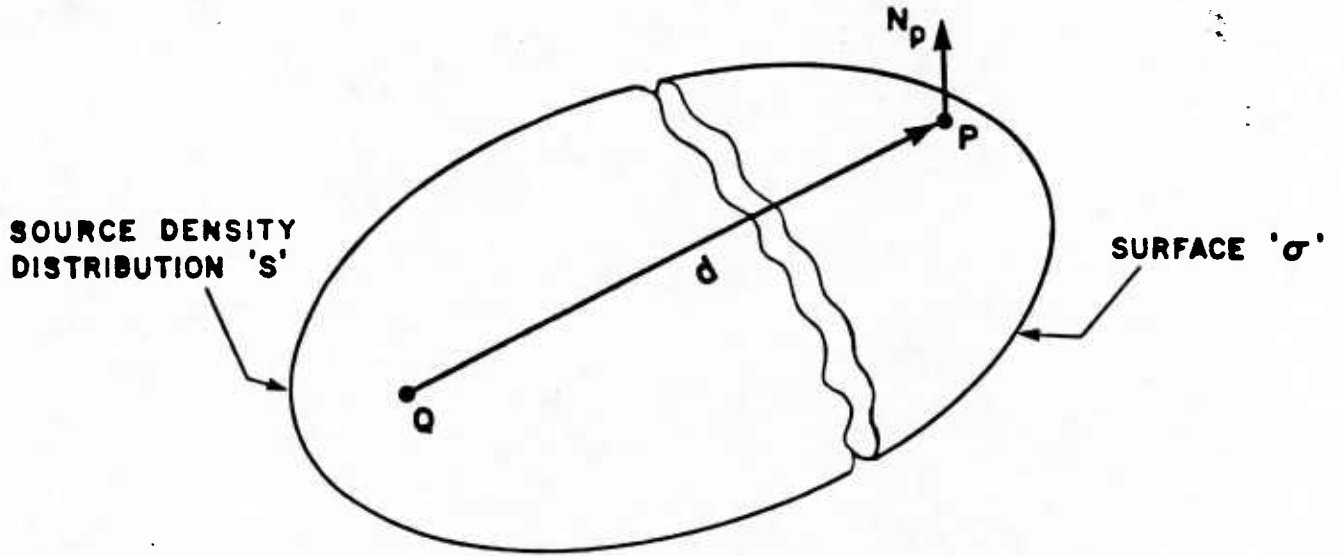


FIG.1 SOURCE AND FIELD POINTS ON A SURFACE

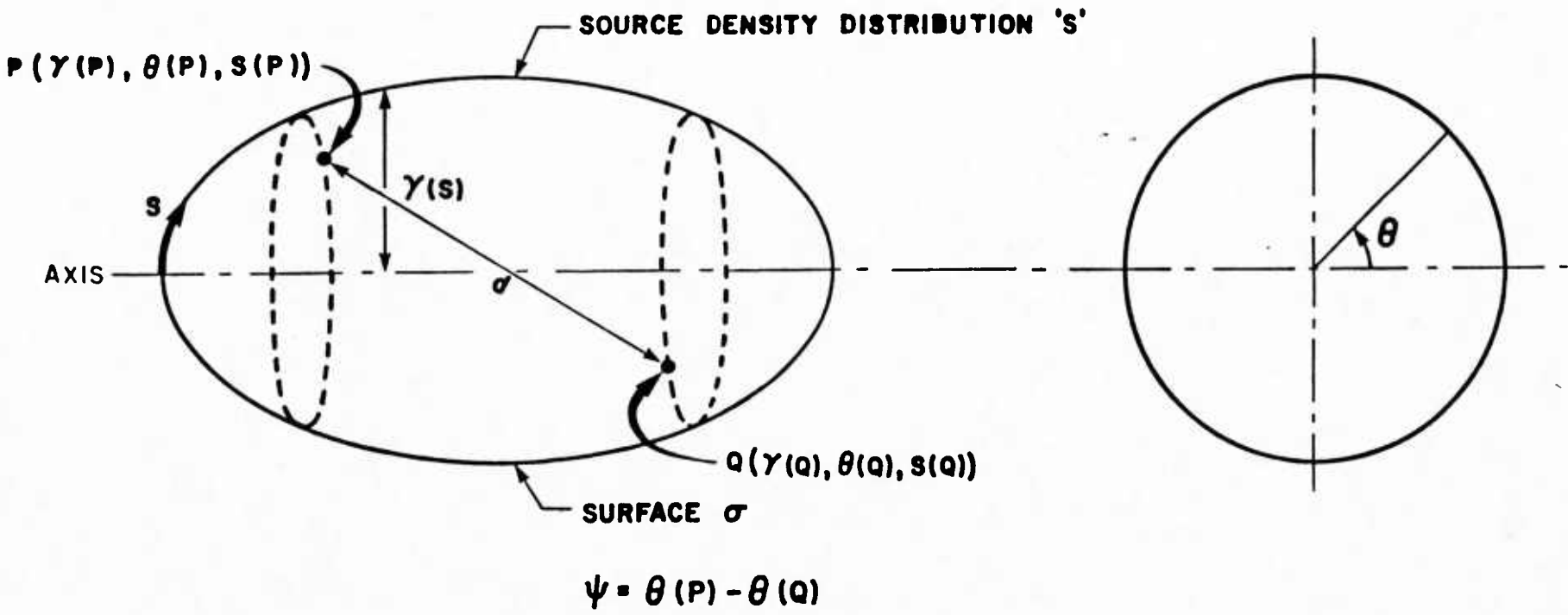


FIG. 2 GEOMETRY OF A SURFACE OF REVOLUTION

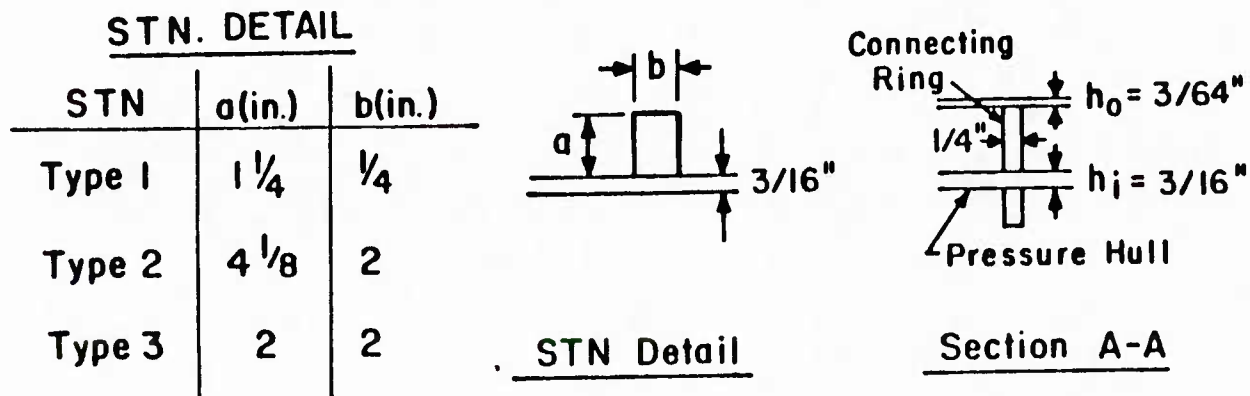
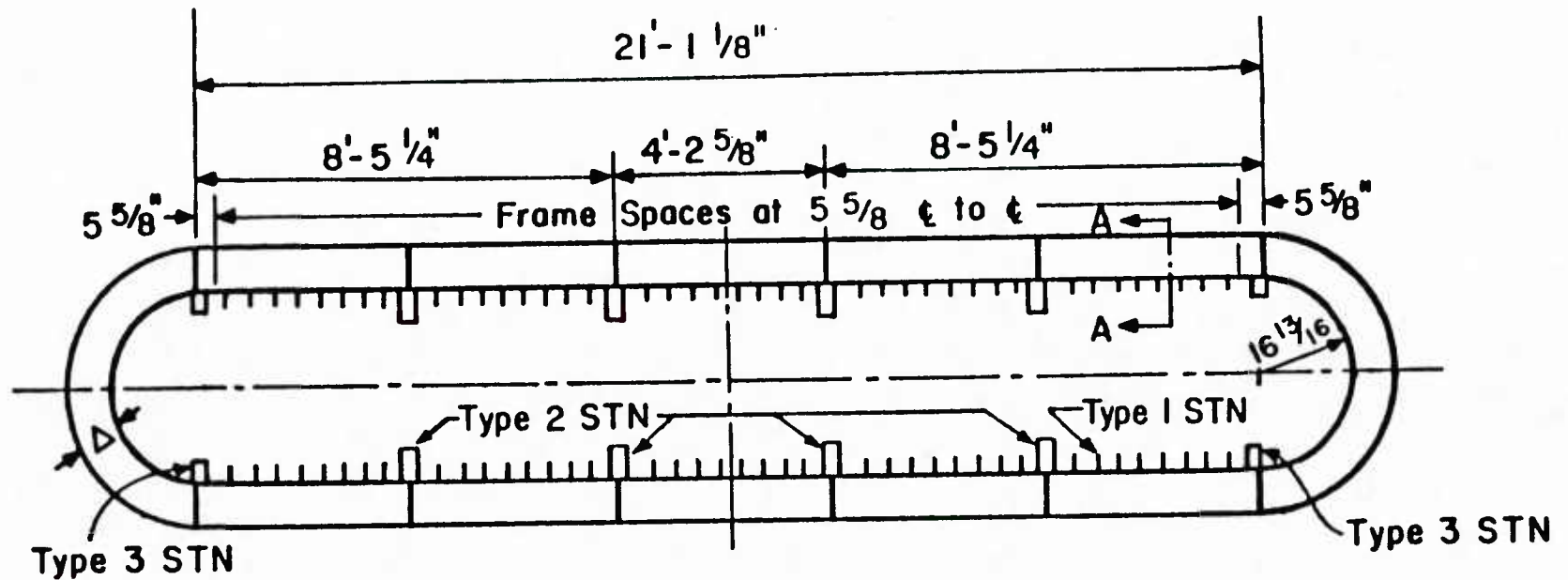


Fig. 3 DOUBLE HULL STRUCTURE

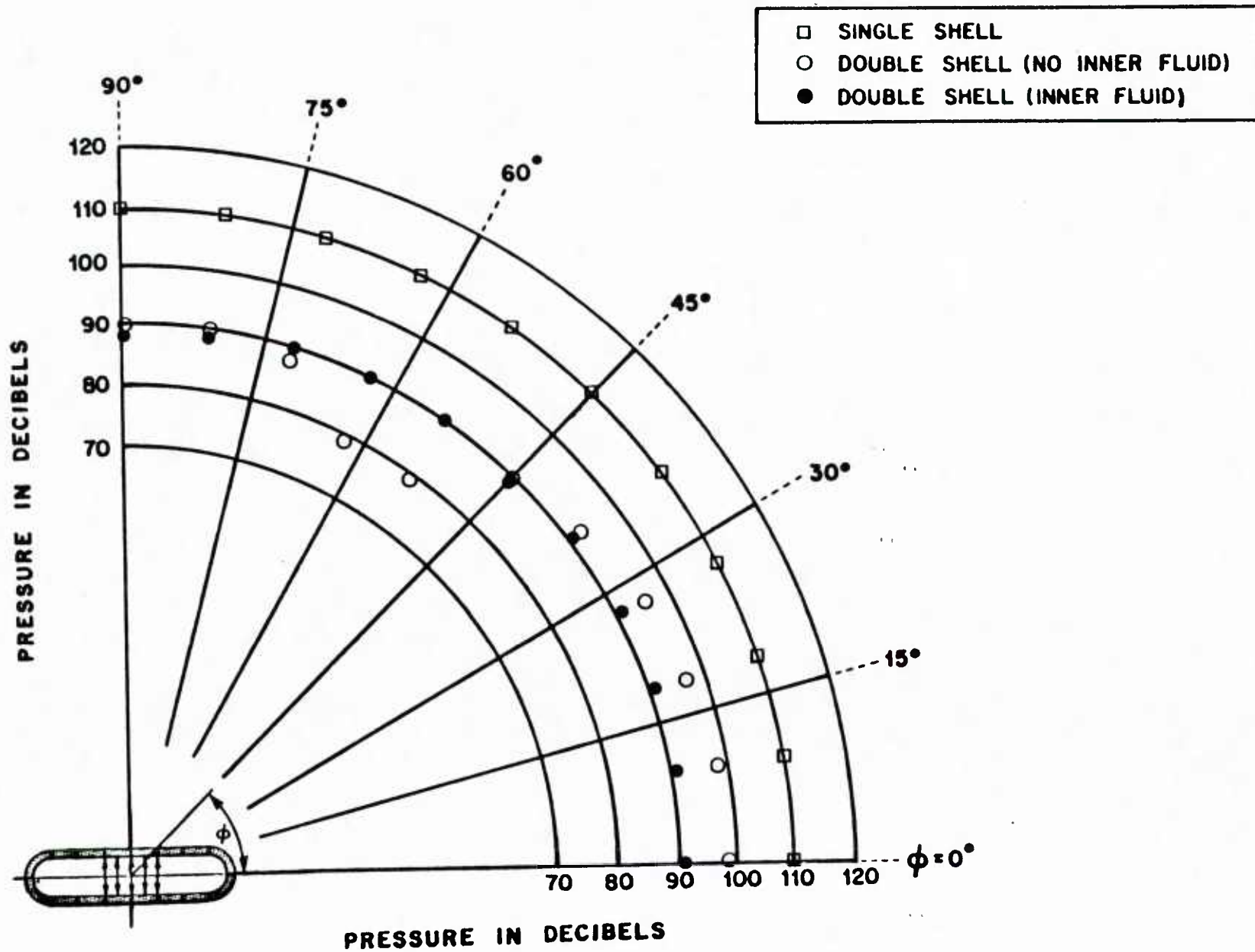


FIG. 5 RADIATED FLUID PRESSURE (dB) AT $\bar{R} = 32$
 AXISYMMETRIC BAND LOAD IN CENTRAL COMPARTMENT;
 $f = 100$ Hz

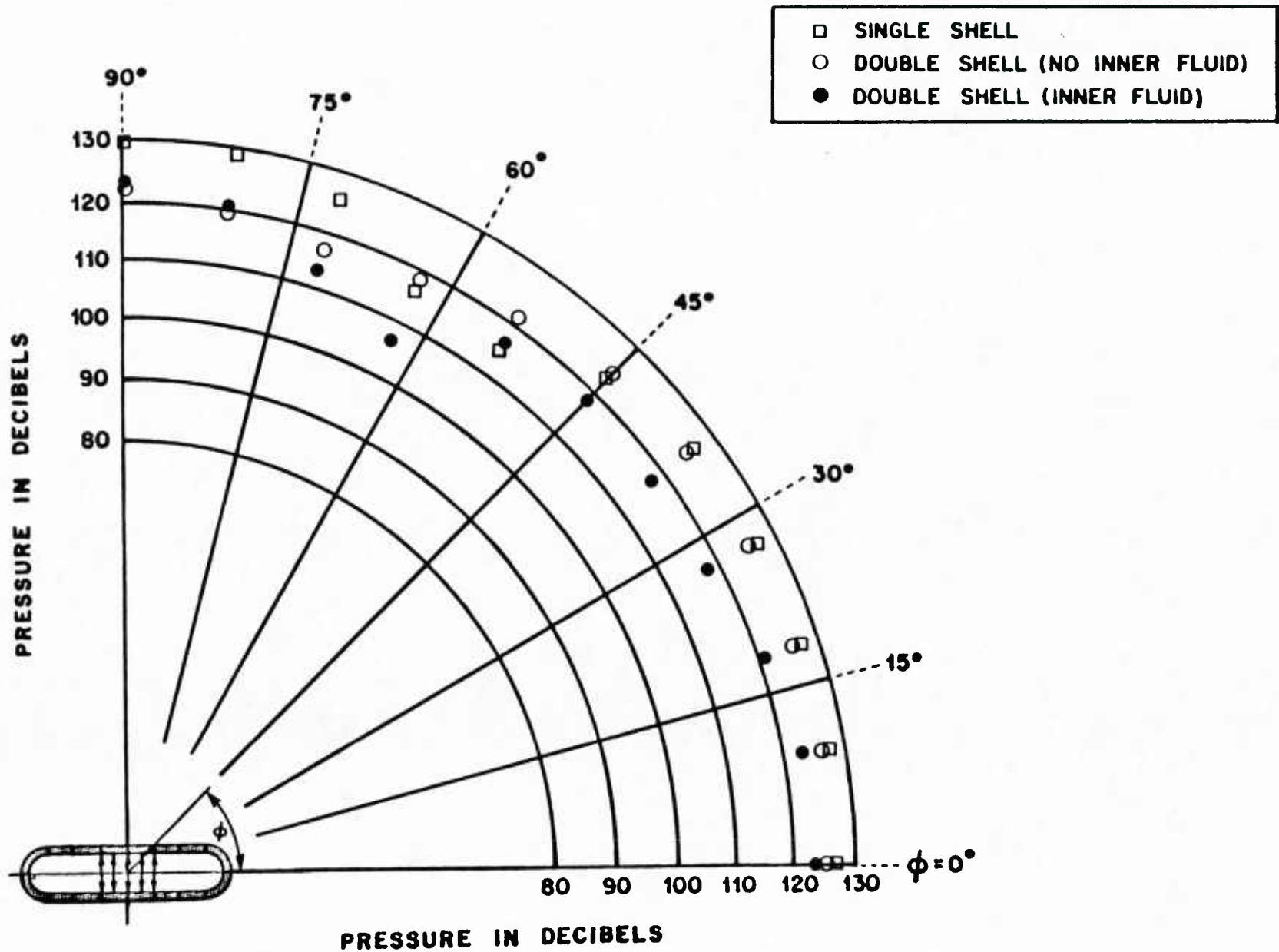


FIG. 6 RADIATED FLUID PRESSURE (dB) AT $\bar{R} = 32$
 AXISYMMETRIC BAND LOAD IN CENTRAL COMPARTMENT;
 $f = 250$ Hz

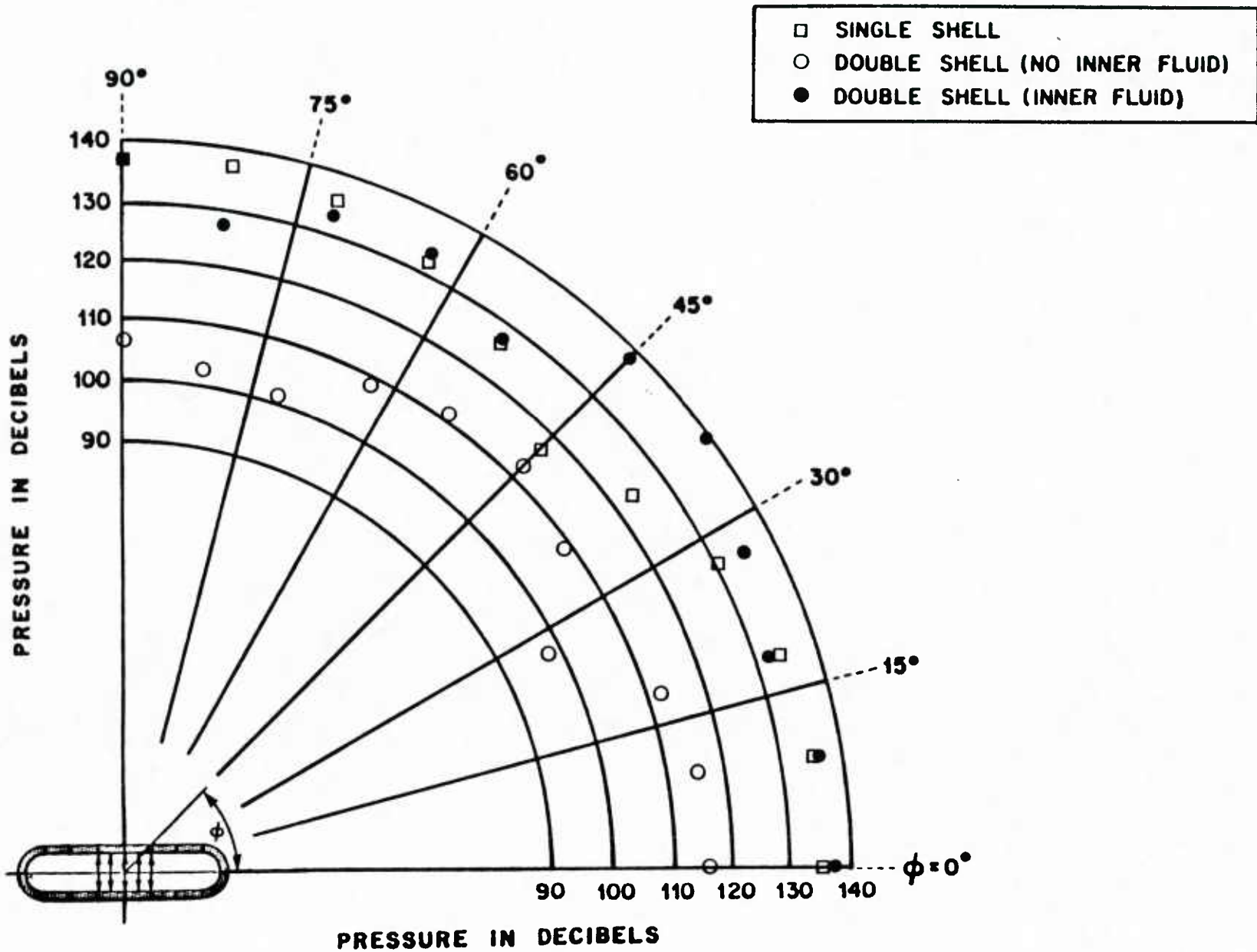


FIG. 7 RADIATED FLUID PRESSURE (dB) AT $\bar{R} = 32$
 AXISYMMETRIC BAND LOAD IN CENTRAL COMPARTMENT;
 $f = 500$ Hz

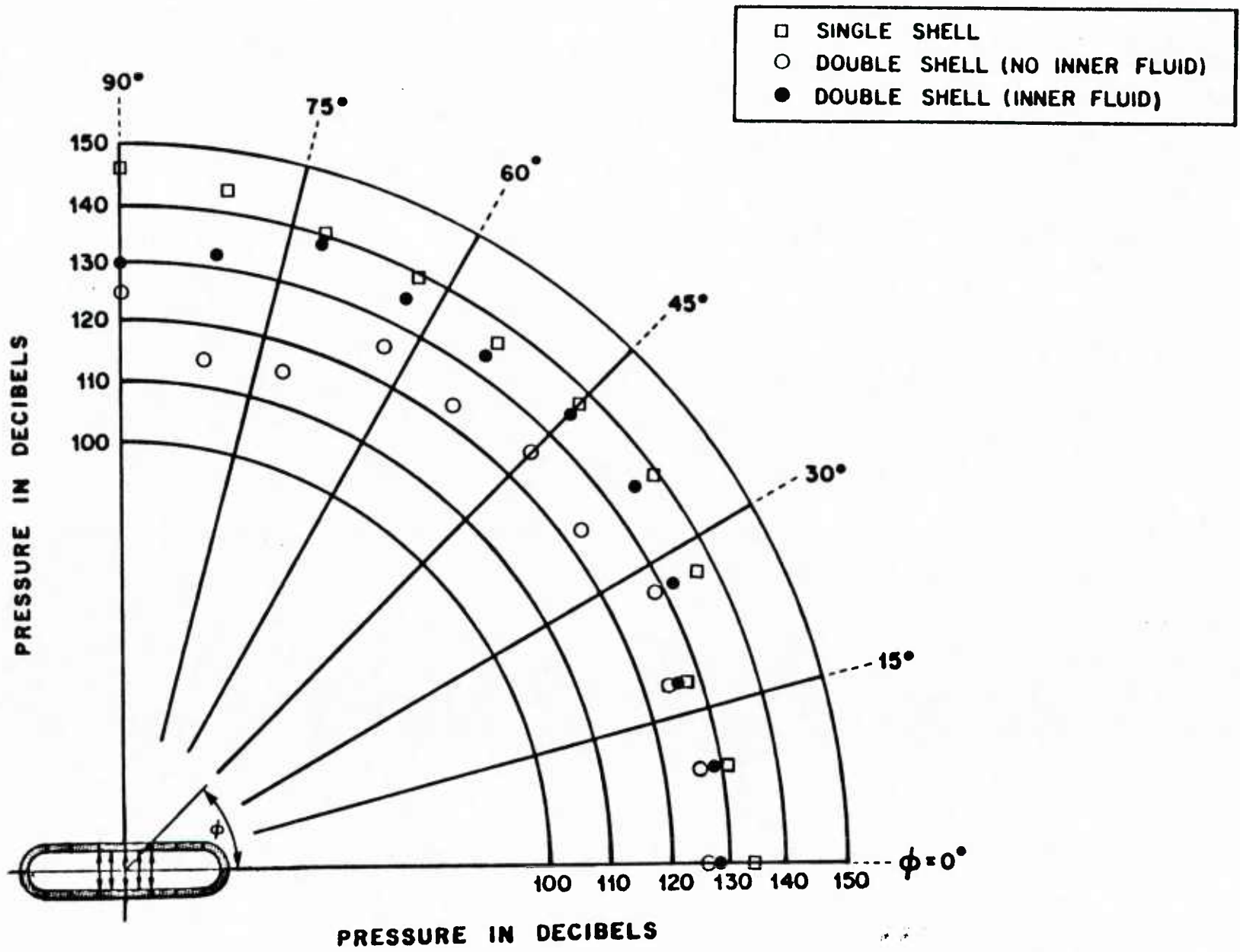


FIG. 8 RADIATED FLUID PRESSURE (dB) AT $\bar{R} = 32$
 AXISYMMETRIC BAND LOAD IN CENTRAL COMPARTMENT;
 $f = 1,000$ Hz

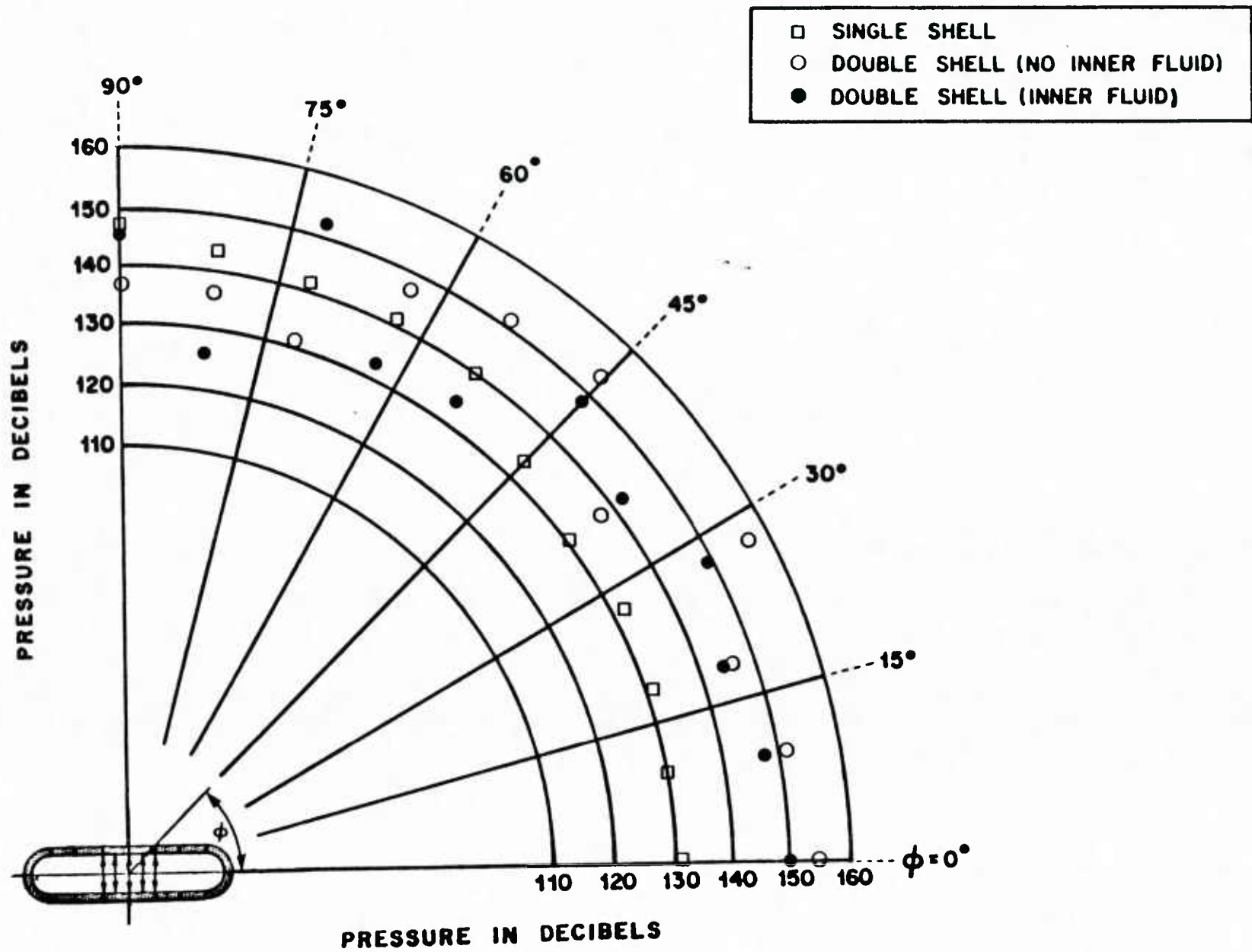


FIG. 9 RADIATED FLUID PRESSURE (dB) AT $\bar{R} = 32$
 AXISYMMETRIC BAND LOAD IN CENTRAL COMPARTMENT;
 $f = 1,500$ Hz

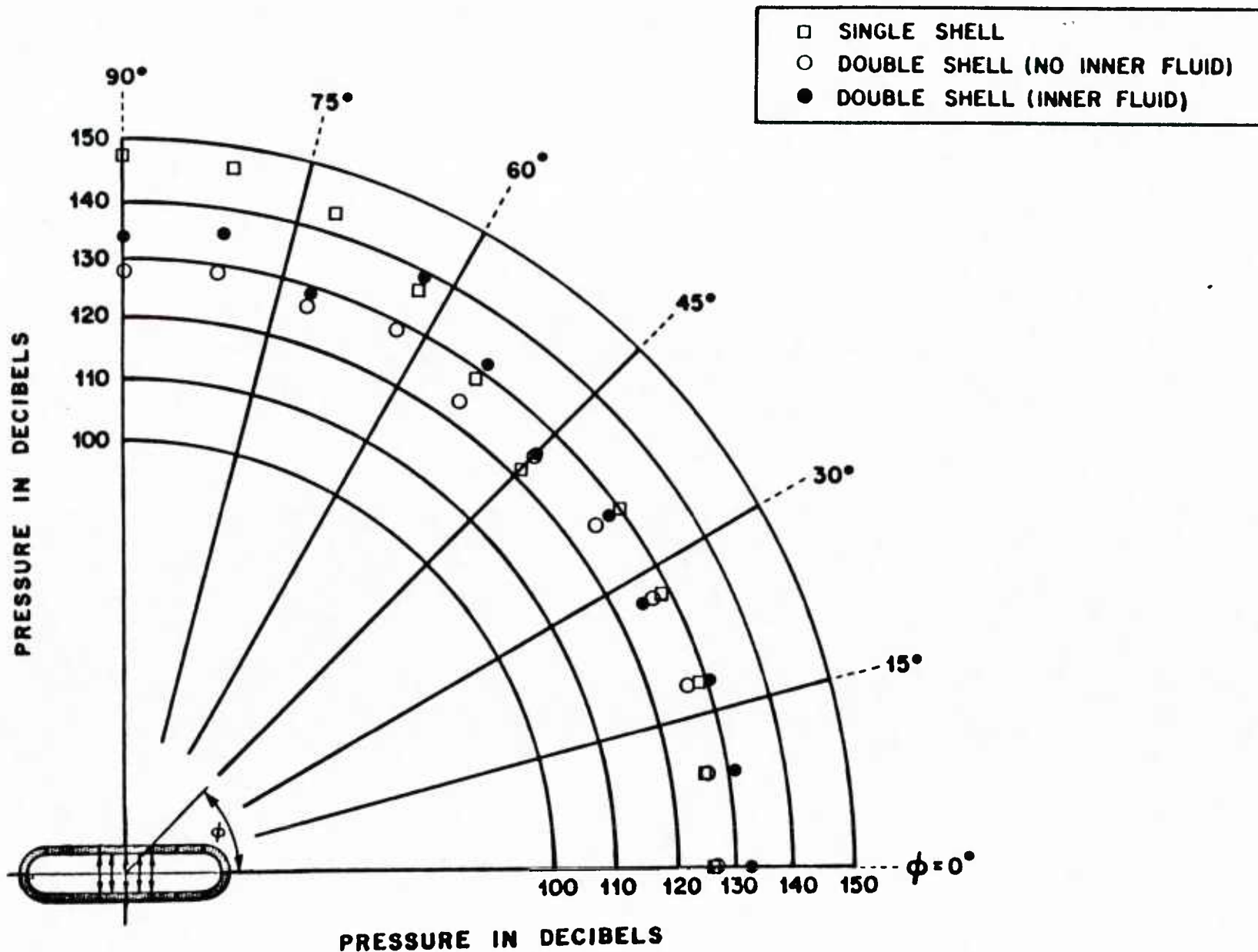


FIG. 10 RADIATED FLUID PRESSURE (dB) AT $\bar{R} = 32$
 AXISYMMETRIC BAND LOAD IN CENTRAL COMPARTMENT;
 $f = 2,000$ Hz

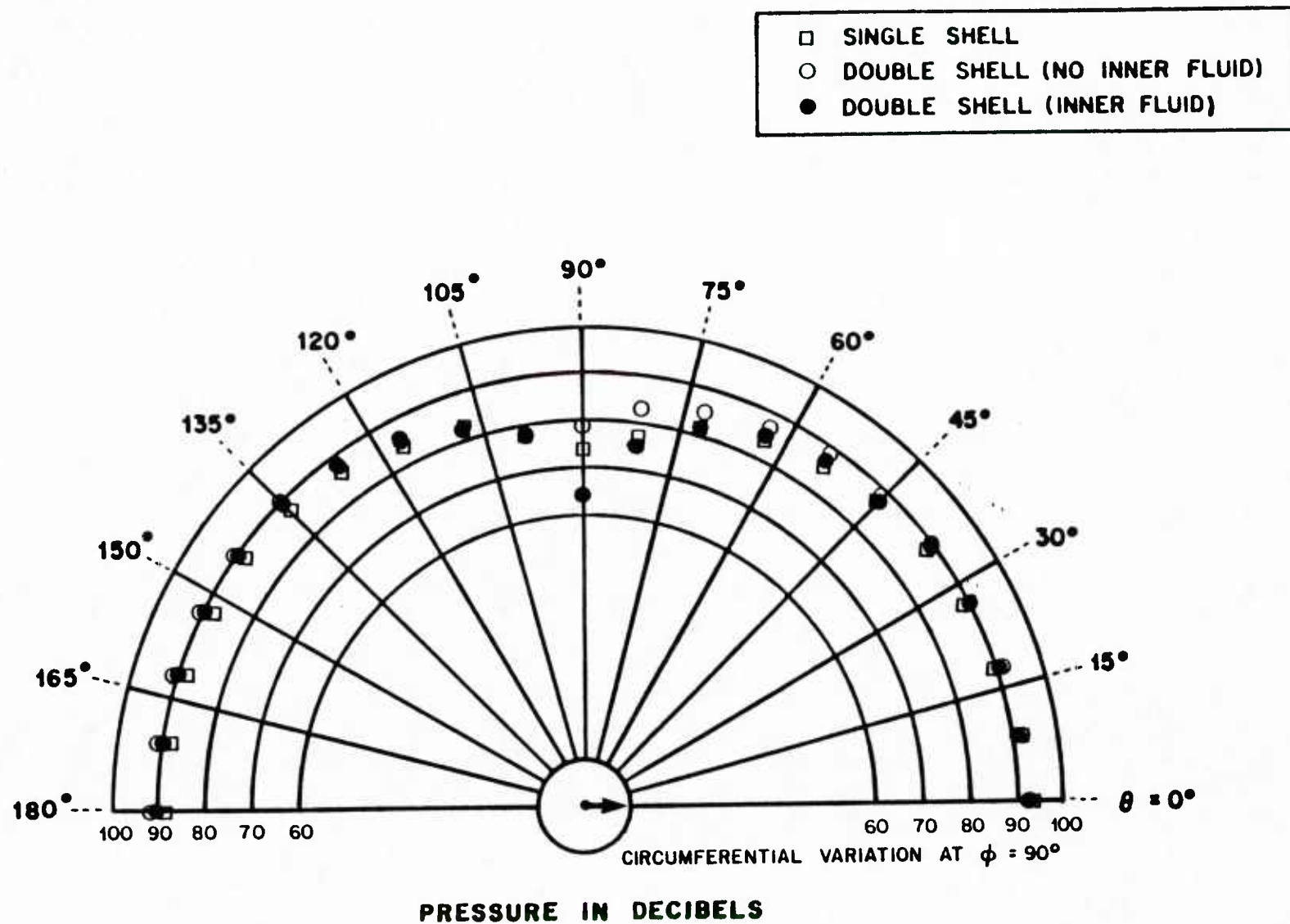


FIG. 11 RADIATED FLUID PRESSURE (dB) AT $\bar{R} = 32$
 LINE LOAD IN CENTRAL COMPARTMENT ; $f = 100$ Hz

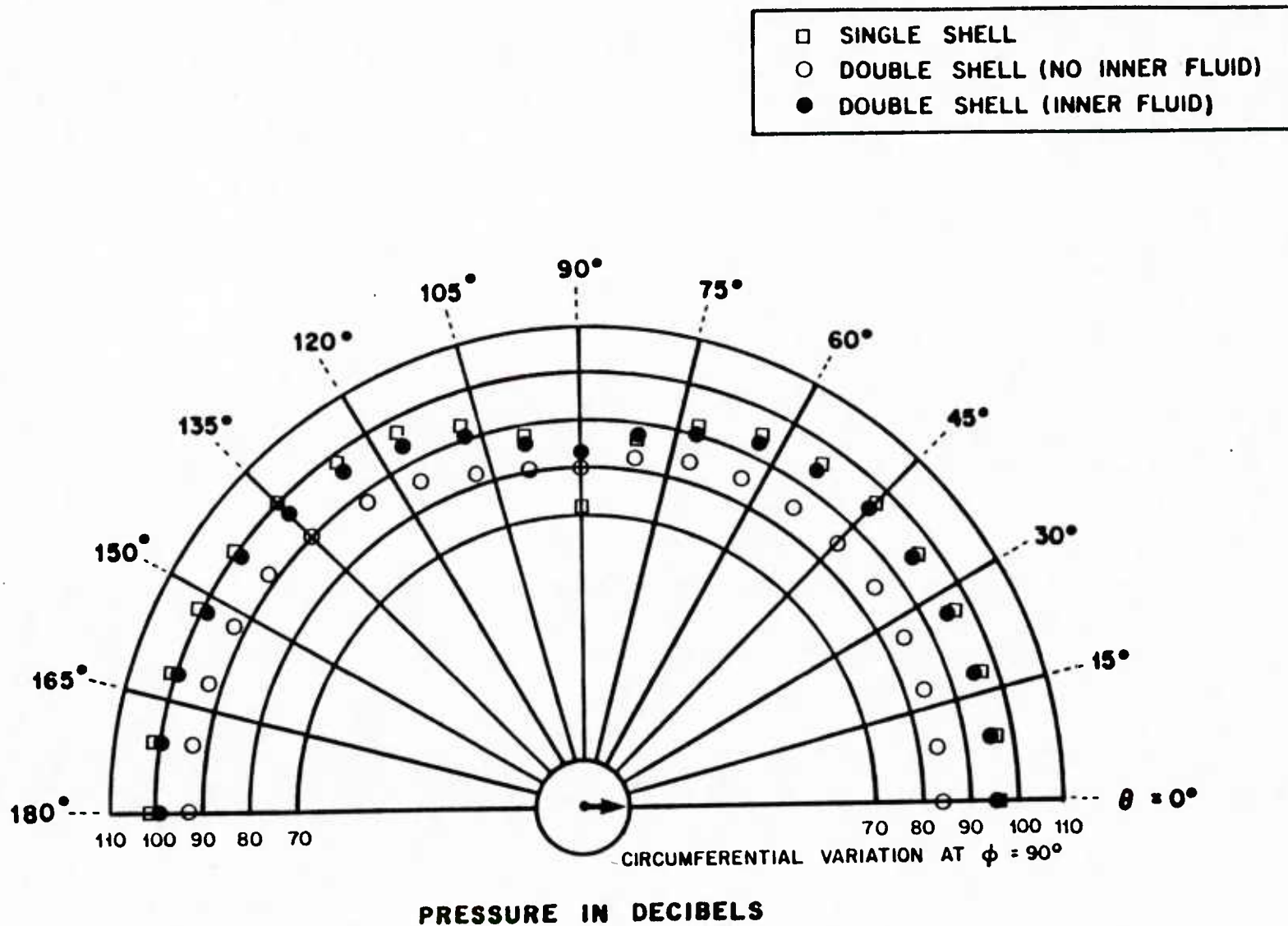
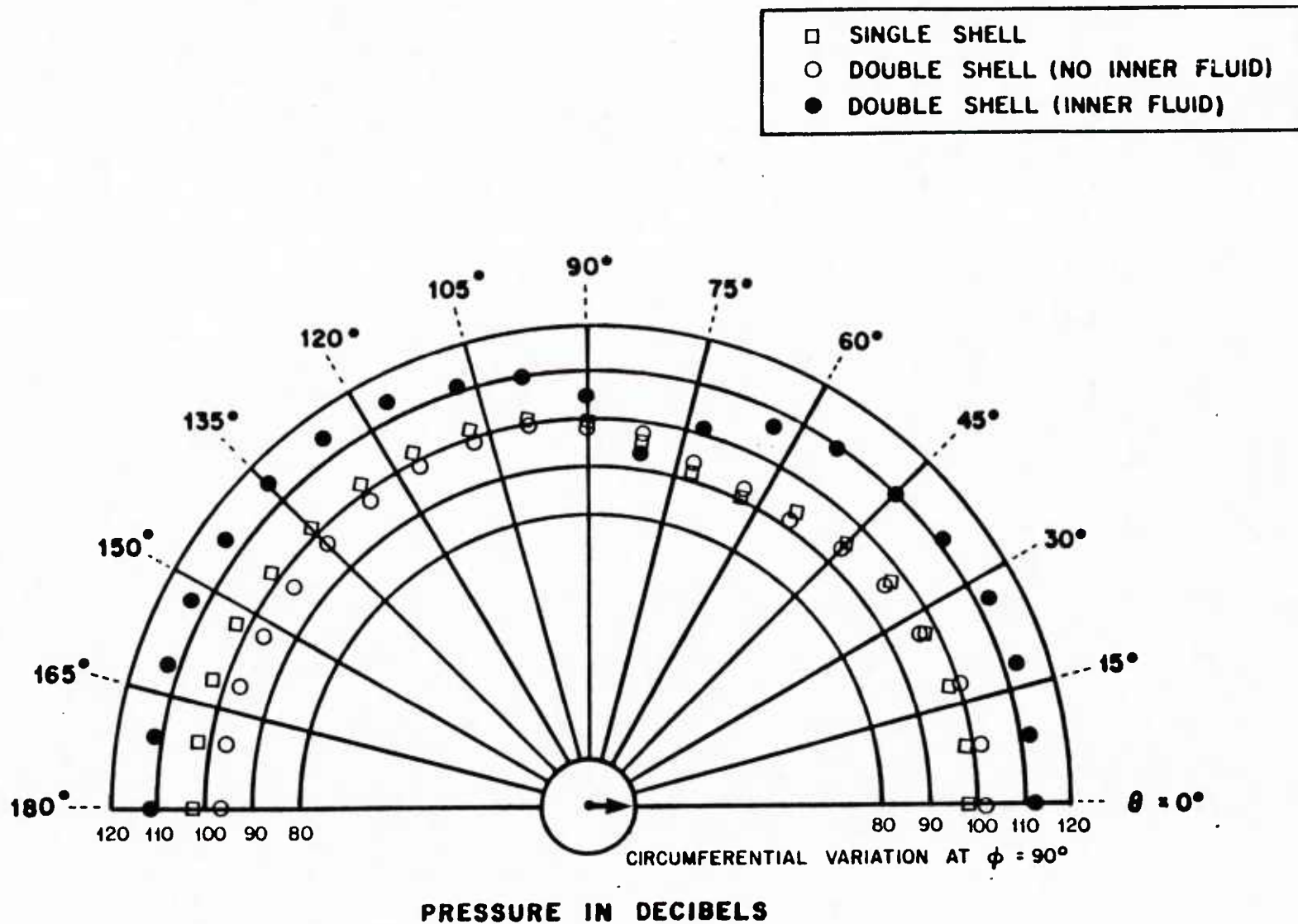


FIG. 12 RADIATED FLUID PRESSURE (dB) AT $\bar{R} = 32$
 LINE LOAD IN CENTRAL COMPARTMENT; $f = 250$ Hz



- SINGLE SHELL
- DOUBLE SHELL (NO INNER FLUID)
- DOUBLE SHELL (INNER FLUID)

FIG. 13 RADIATED FLUID PRESSURE (dB) AT $\bar{R} = 32$
 LINE LOAD IN CENTRAL COMPARTMENT; $f = 500$ Hz

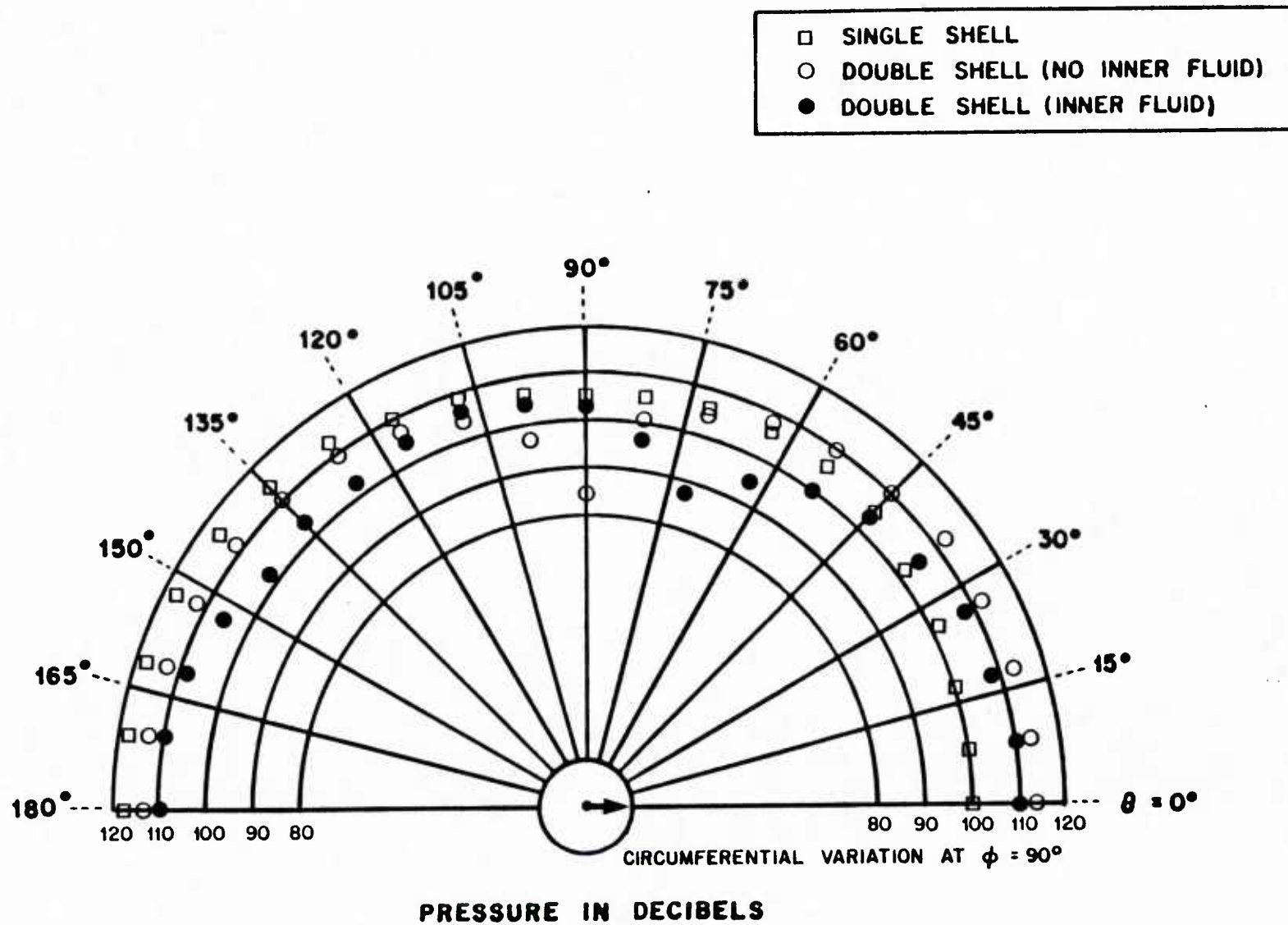


FIG. 14 RADIATED FLUID PRESSURE (dB) AT $\bar{R} = 32$
 LINE LOAD IN CENTRAL COMPARTMENT; $f = 1,000$ Hz

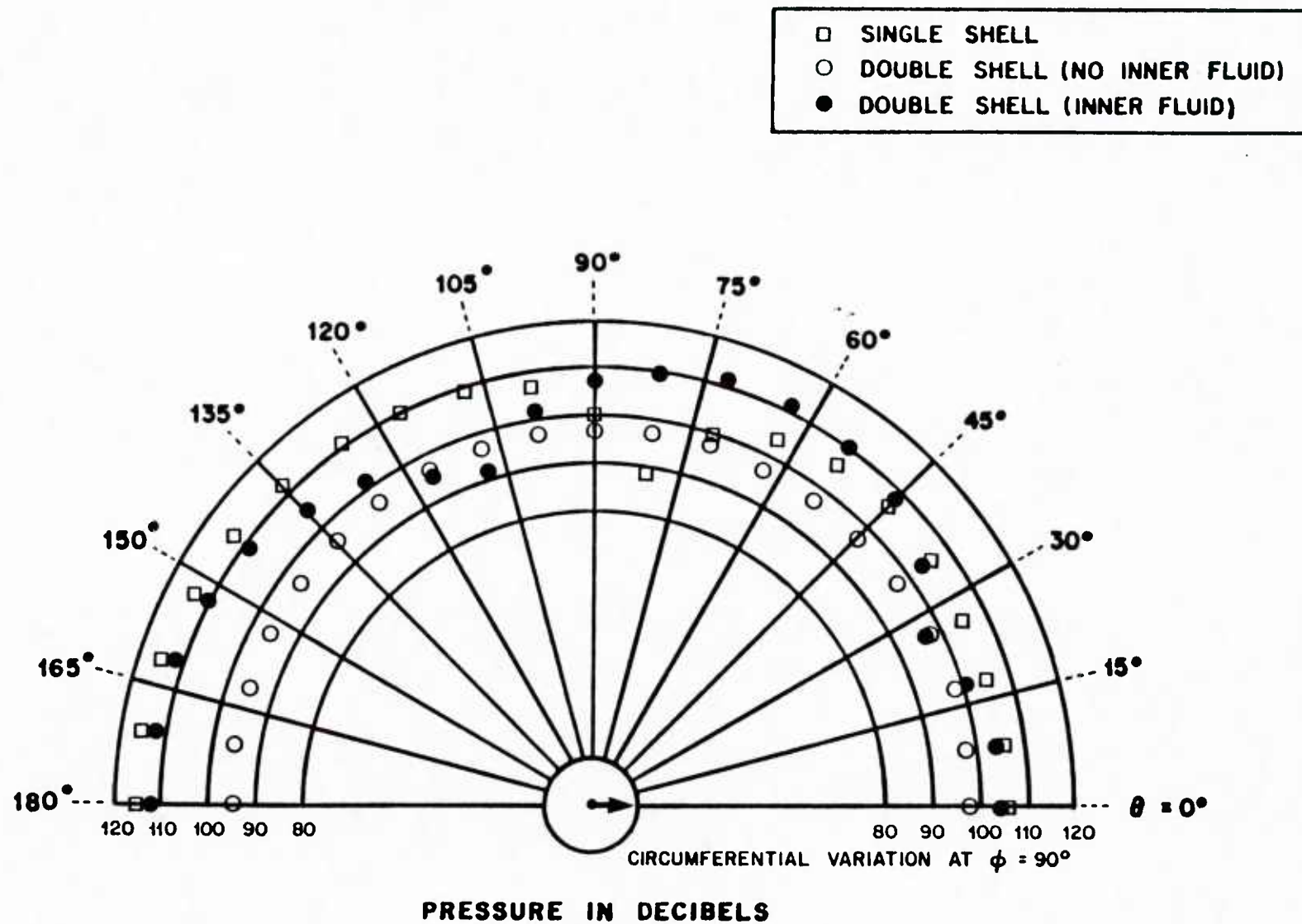


FIG. 15 RADIATED FLUID PRESSURE (dB) AT $\bar{R} = 32$
 LINE LOAD IN CENTRAL COMPARTMENT; $f = 1500$ Hz

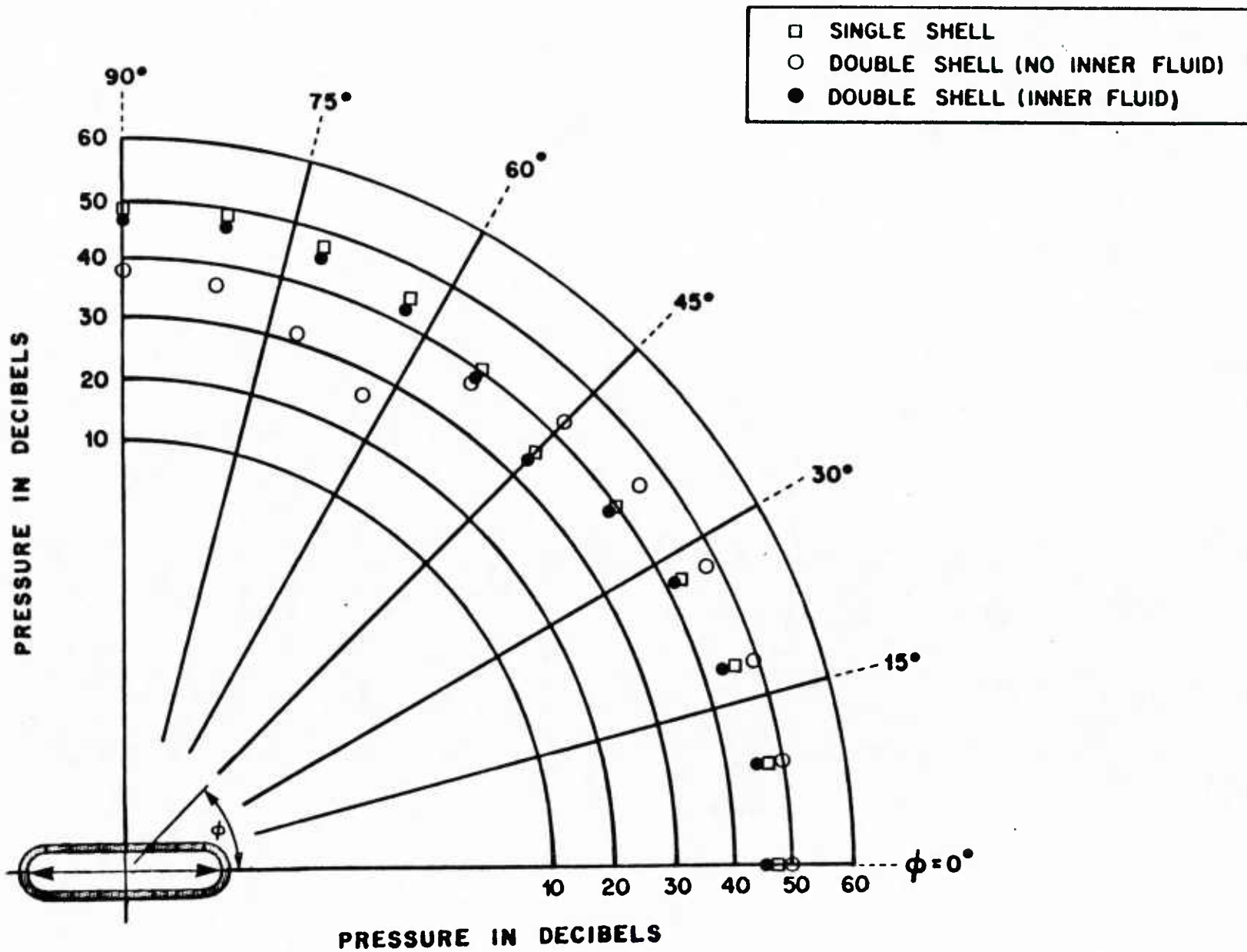


FIG. 16 RADIATED FLUID PRESSURE (dB) AT $\bar{R} = 32$
 CONCENTRATED LOAD ON ENCLOSURES ; $f = 100$ Hz

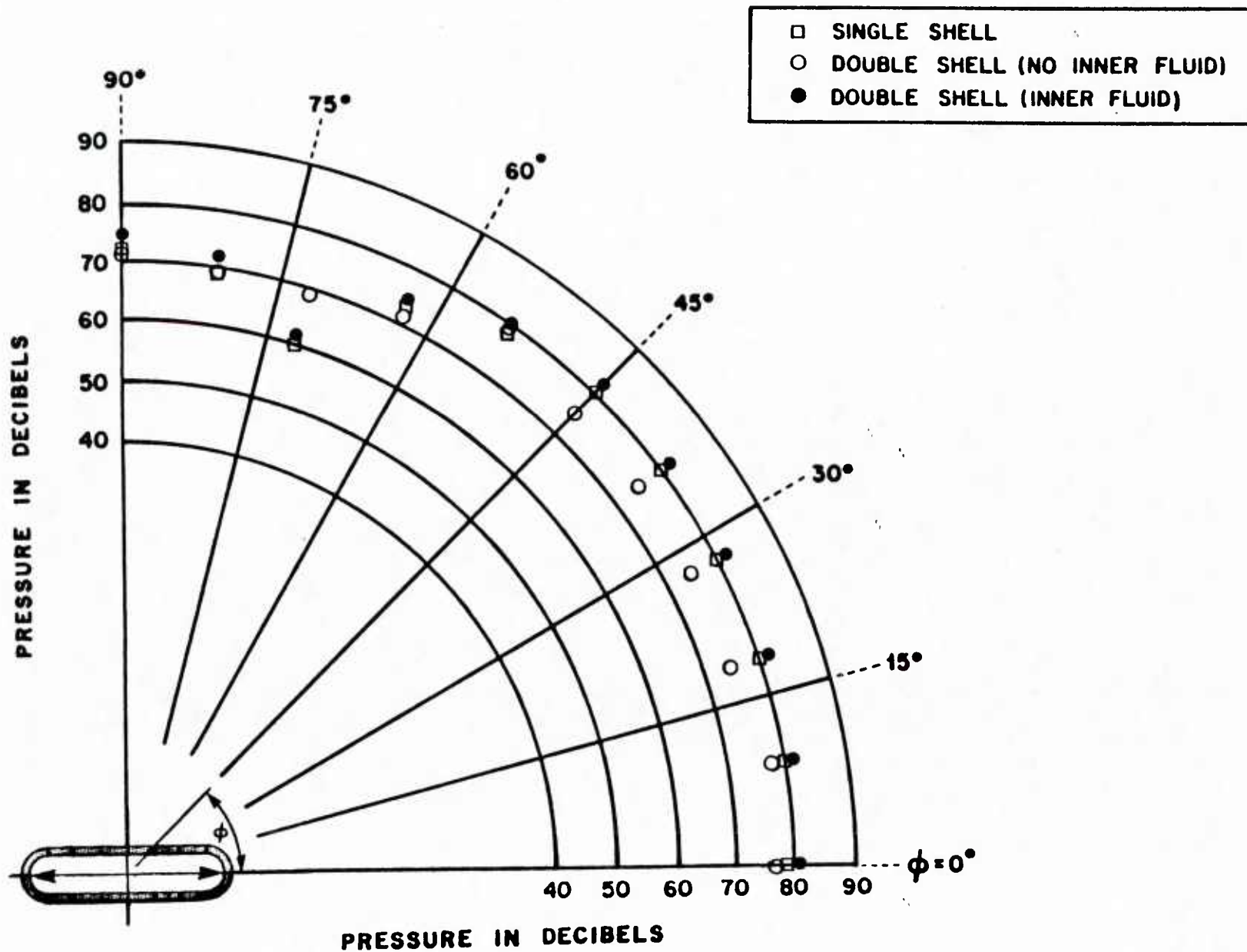


FIG. 17 RADIATED FLUID PRESSURE (dB) AT $\bar{R} = 32$
 CONCENTRATED LOAD ON ENCLOSURES; $f = 250$ Hz

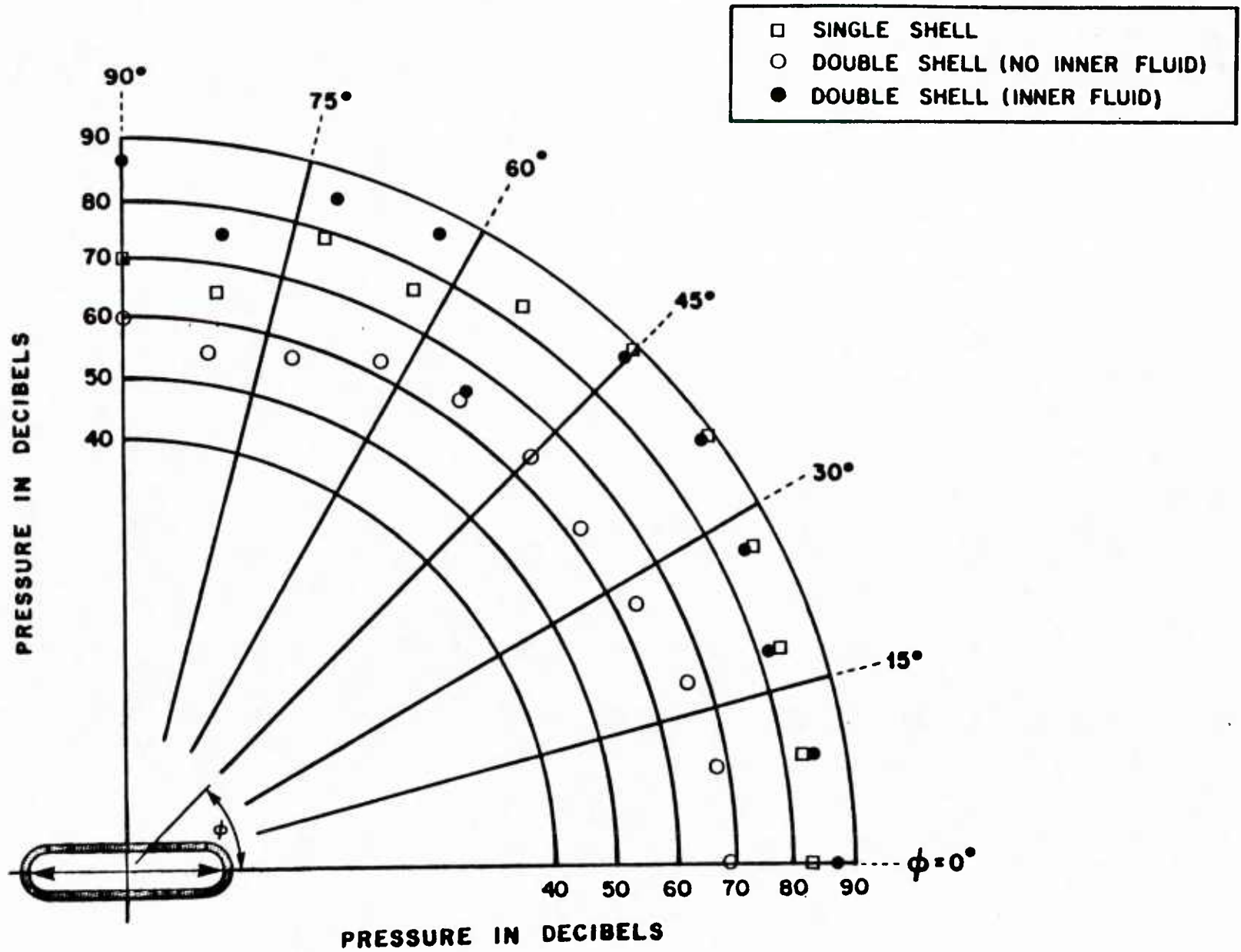


FIG. 18 RADIATED FLUID PRESSURE (dB) AT $\bar{R} = 32$
 CONCENTRATED LOAD ON ENCLOSURES; $f = 500$ Hz

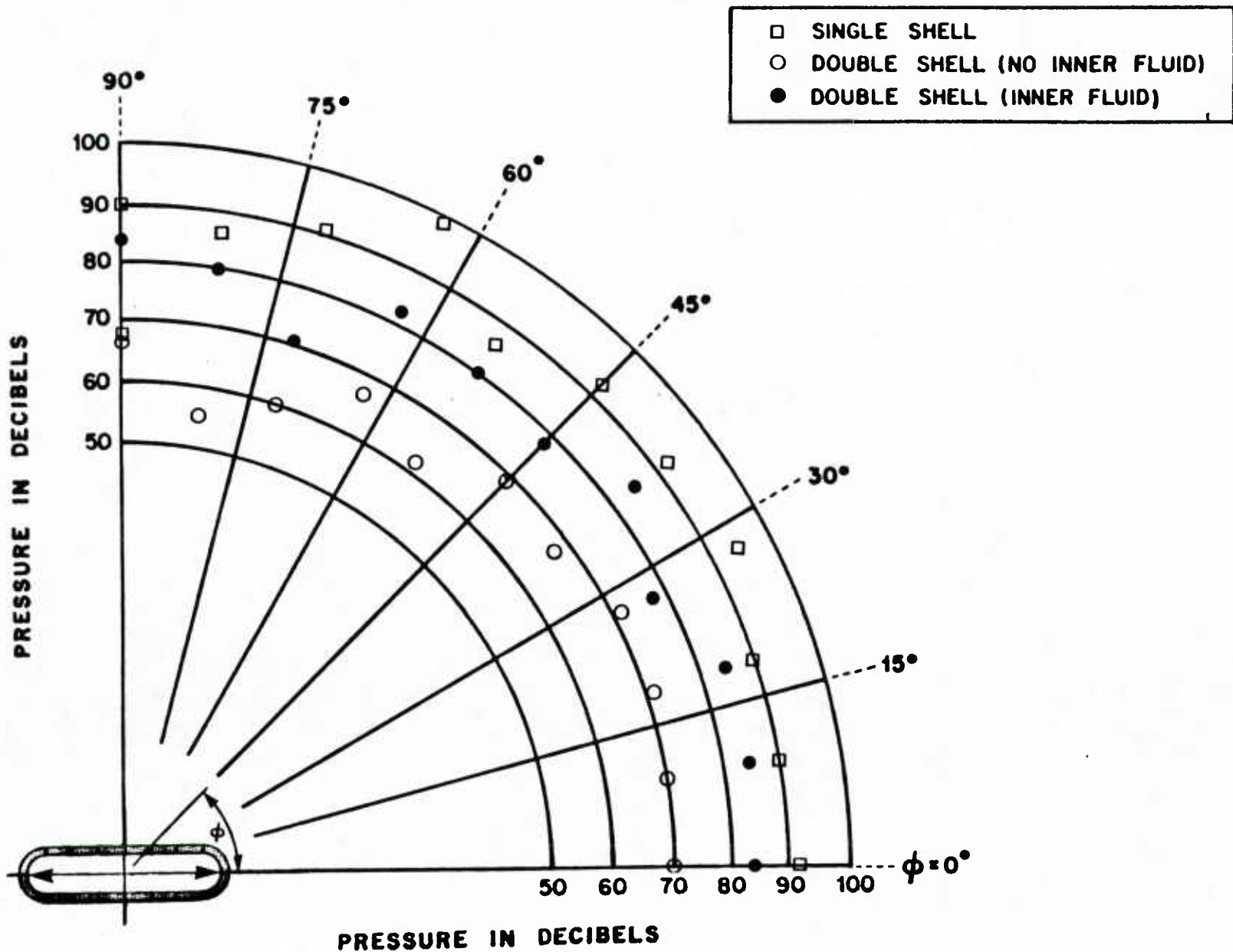


FIG. 19 RADIATED FLUID PRESSURE (dB) AT $\bar{R} = 32$
 CONCENTRATED LOAD ON ENCLOSURES; $f = 1,000$ Hz

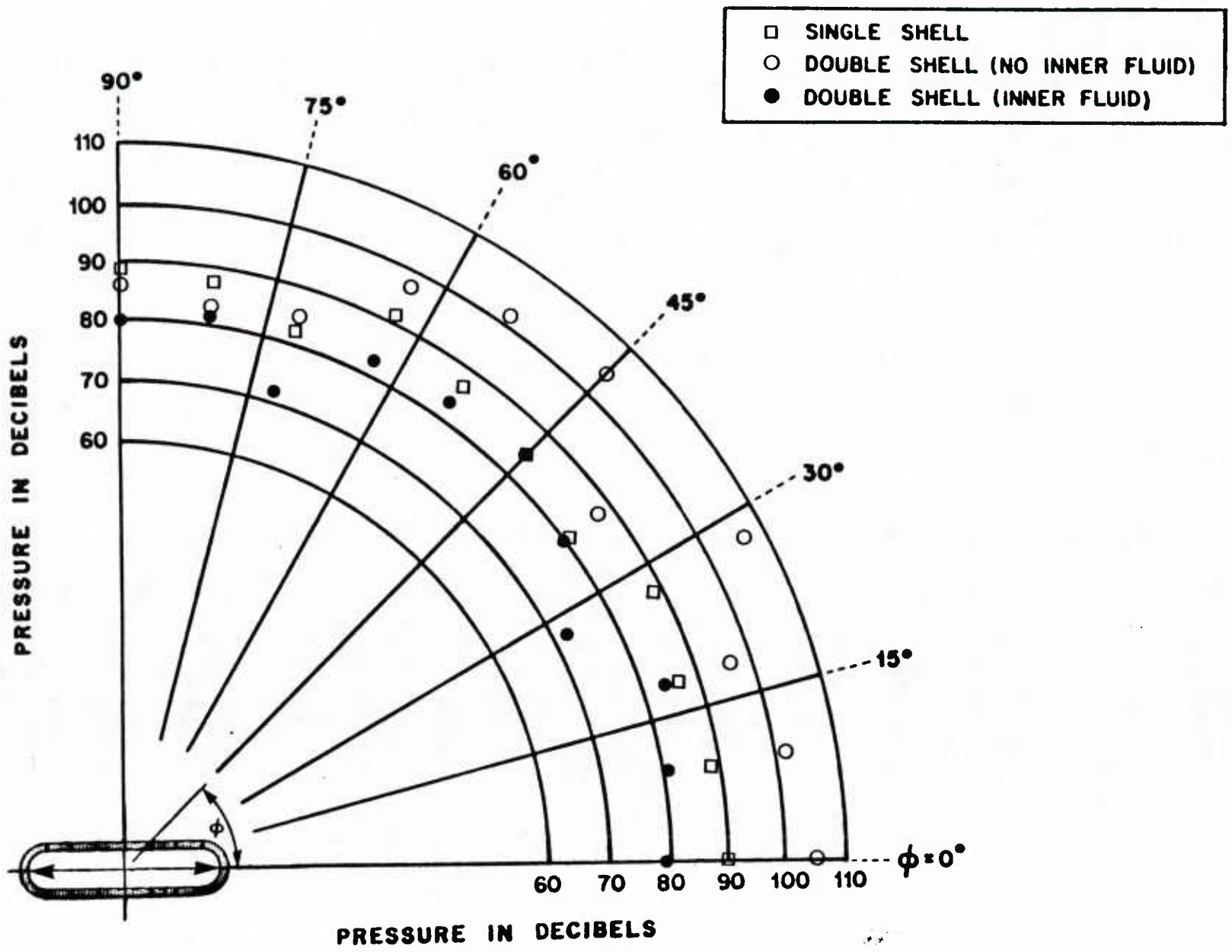


FIG. 20 RADIATED FLUID PRESSURE (dB) AT $\bar{R} = 32$
 CONCENTRATED LOAD ON ENCLOSURES ; $f = 1,500$ Hz

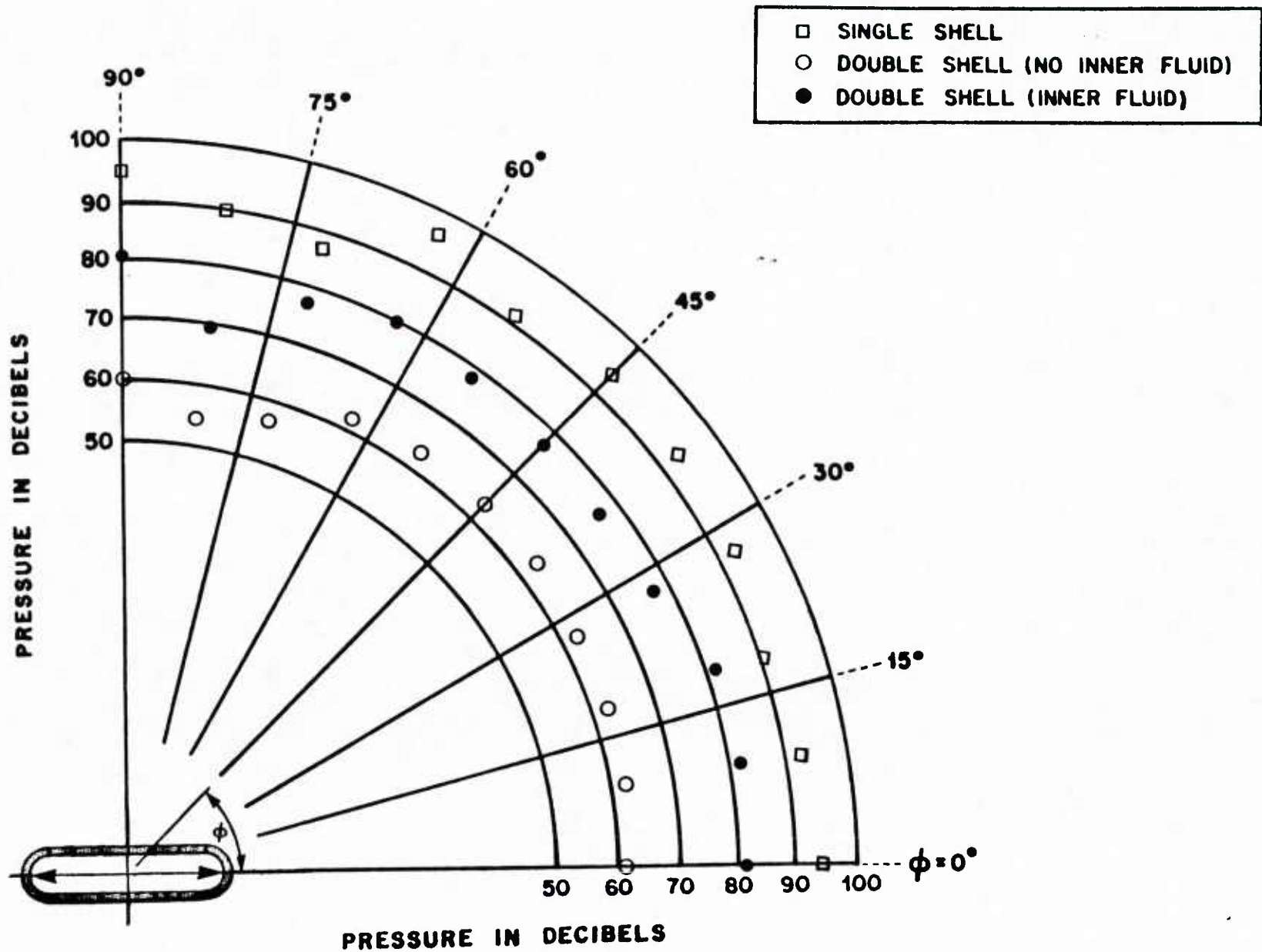


FIG. 21 RADIATED FLUID PRESSURE (dB) AT $\bar{R} = 32$
 CONCENTRATED LOAD ON ENCLOSURES; $f = 2,000$ Hz

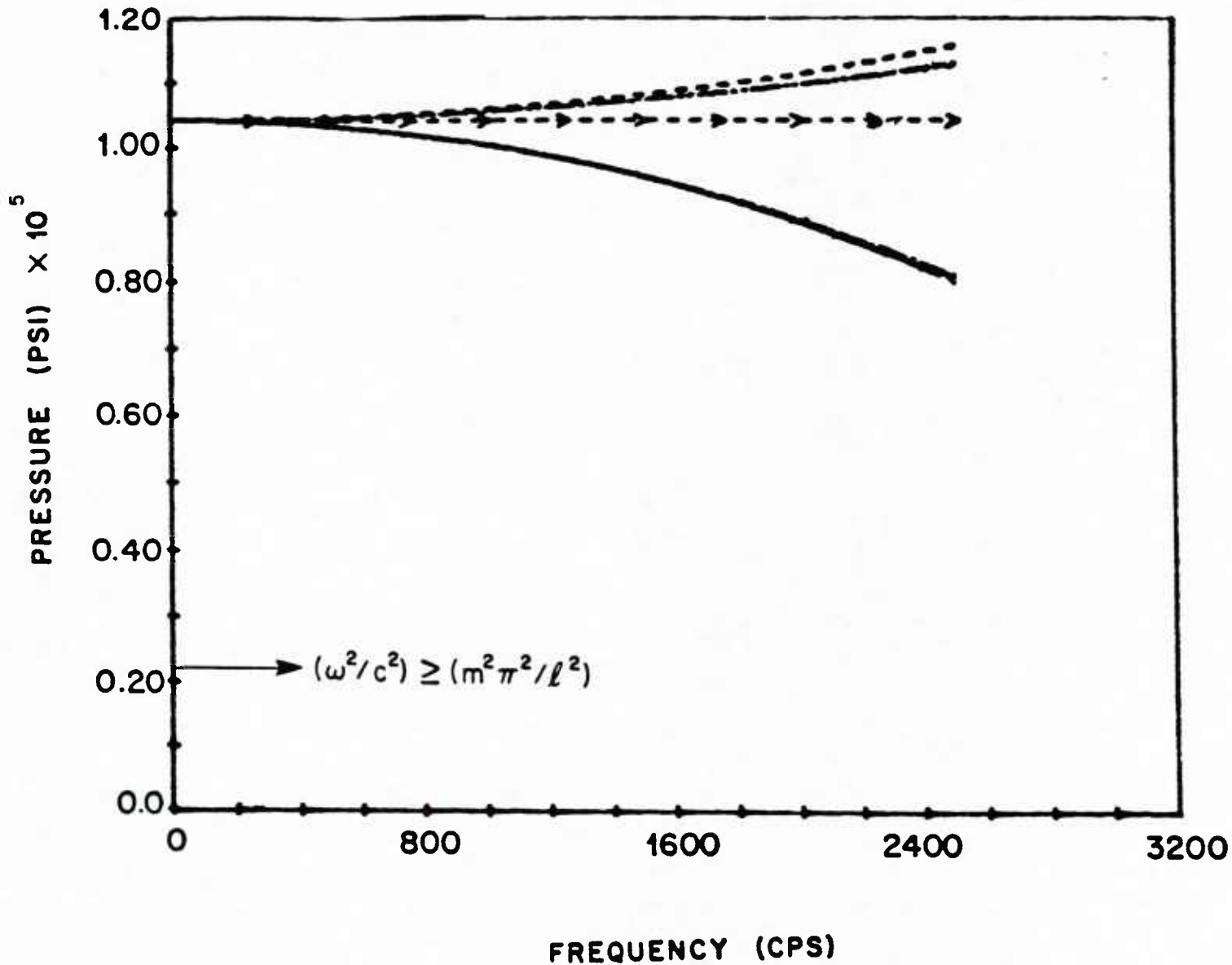
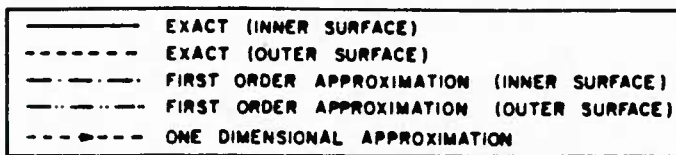


FIG. 22 COMPARISON OF PRESSURES OBTAINED FROM EXACT AND APPROXIMATE SOLUTIONS (n = 0 , m = 0)

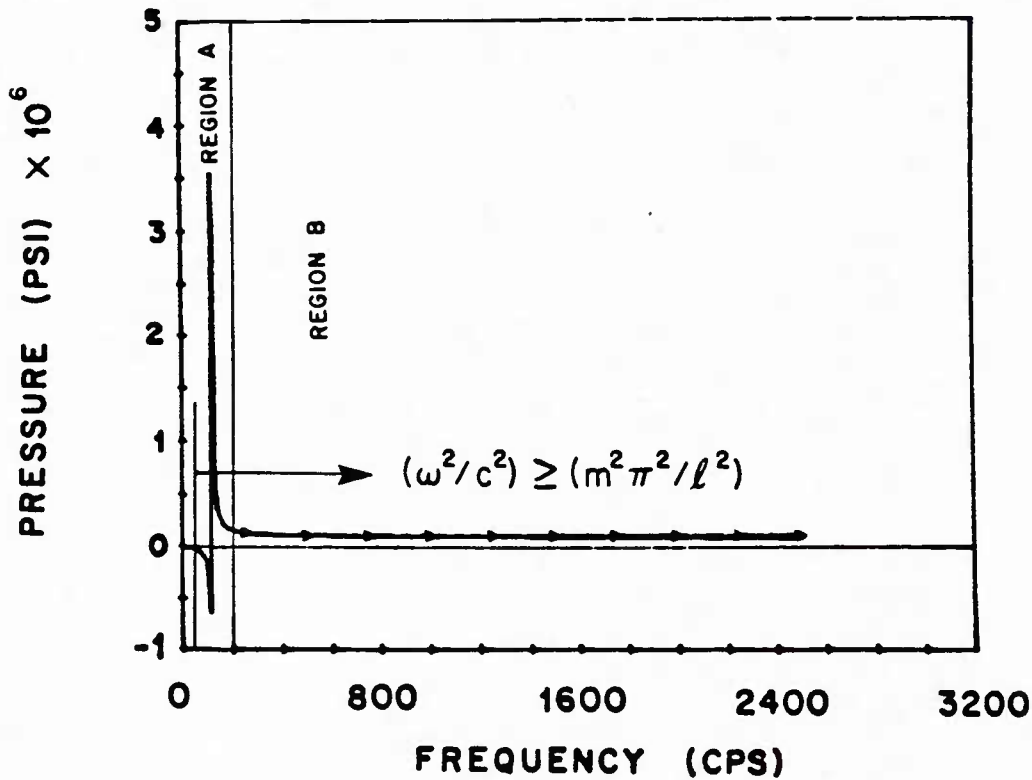
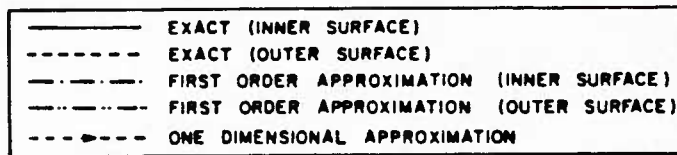
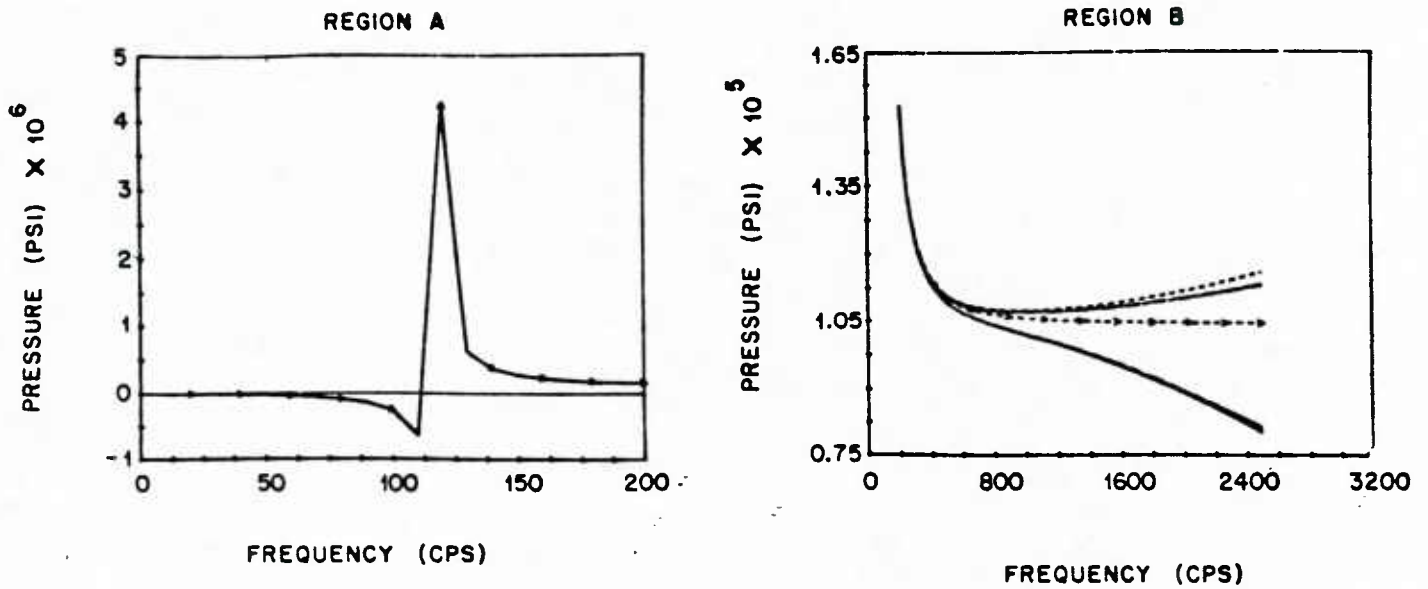
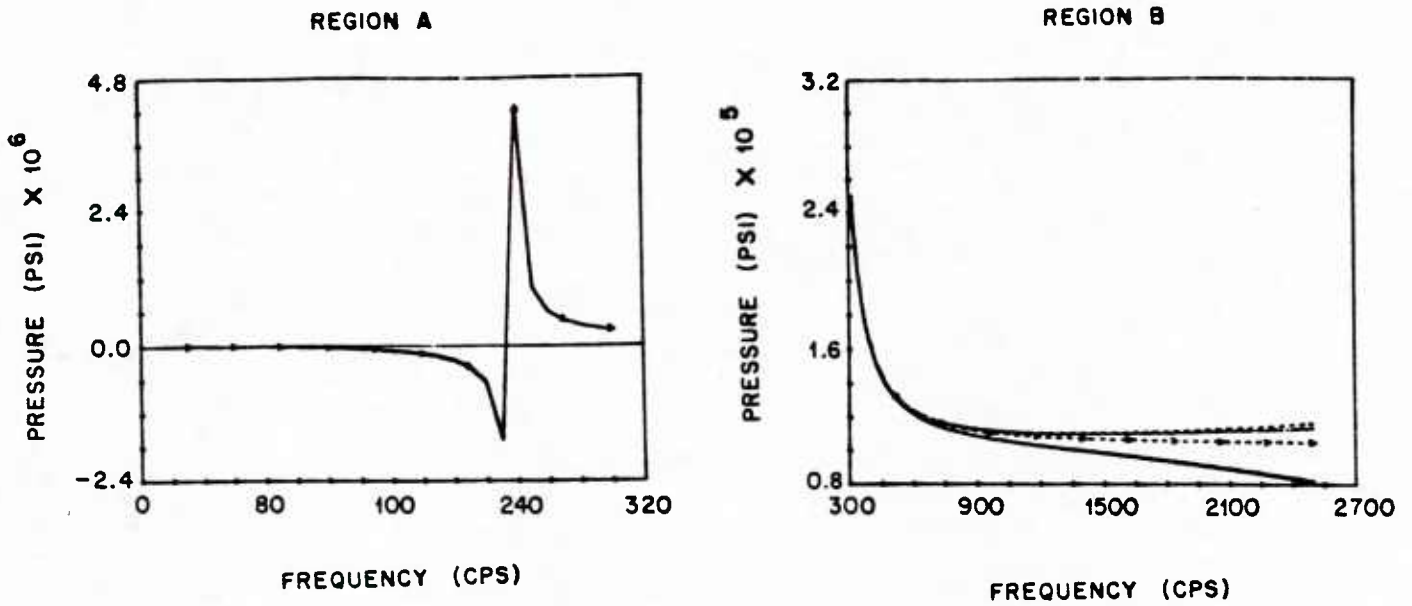


FIG. 23 COMPARISON OF PRESSURES OBTAINED FROM EXACT AND APPROXIMATE SOLUTIONS (n = 0 , m = 1)



- EXACT (INNER SURFACE)
- - - EXACT (OUTER SURFACE)
- · - · - FIRST ORDER APPROXIMATION (INNER SURFACE)
- · - · - FIRST ORDER APPROXIMATION (OUTER SURFACE)
- - - > ONE DIMENSIONAL APPROXIMATION

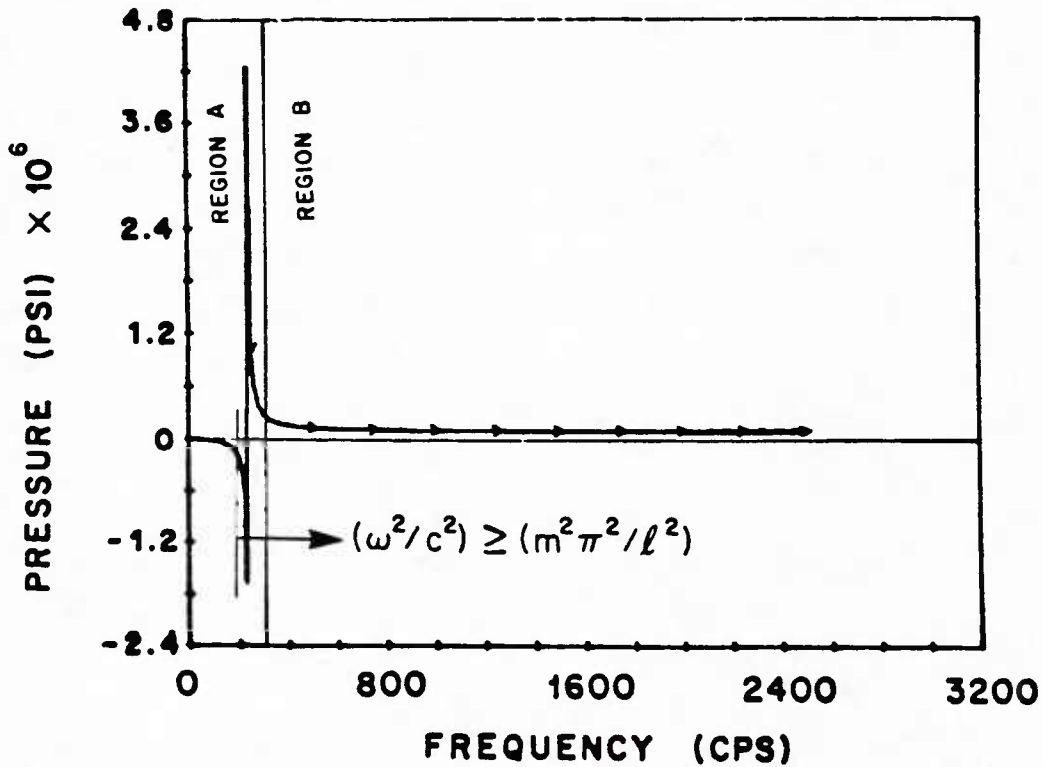


FIG. 24 COMPARISON OF PRESSURES OBTAINED FROM EXACT AND APPROXIMATE SOLUTIONS (n = 0 , m = 2)

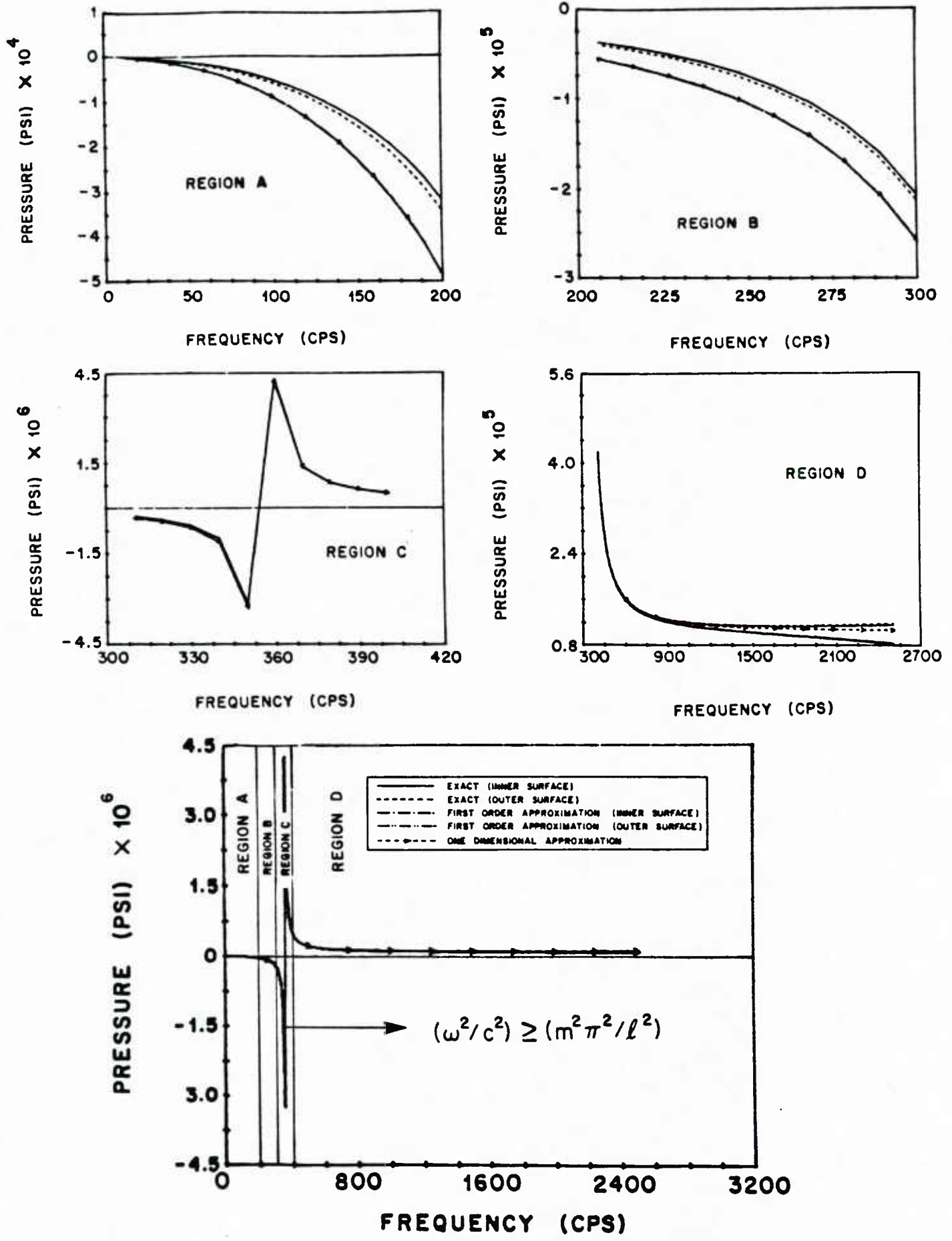


FIG. 25 COMPARISON OF PRESSURES OBTAINED FROM EXACT AND APPROXIMATE SOLUTIONS (n = 0, m = 3)

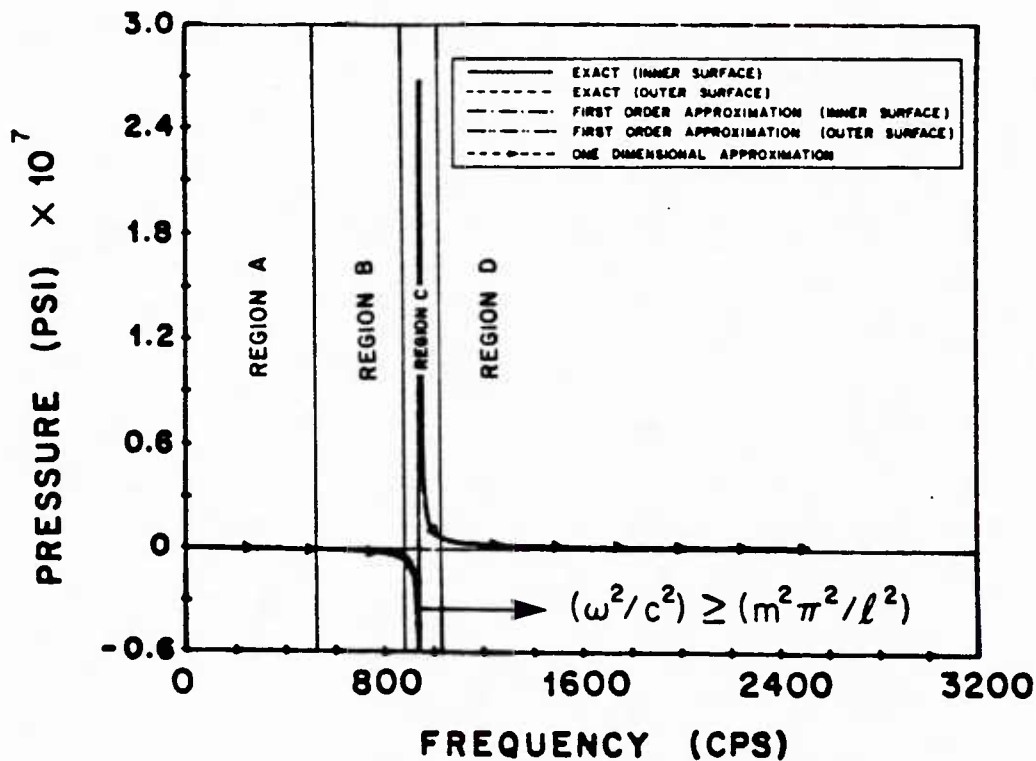
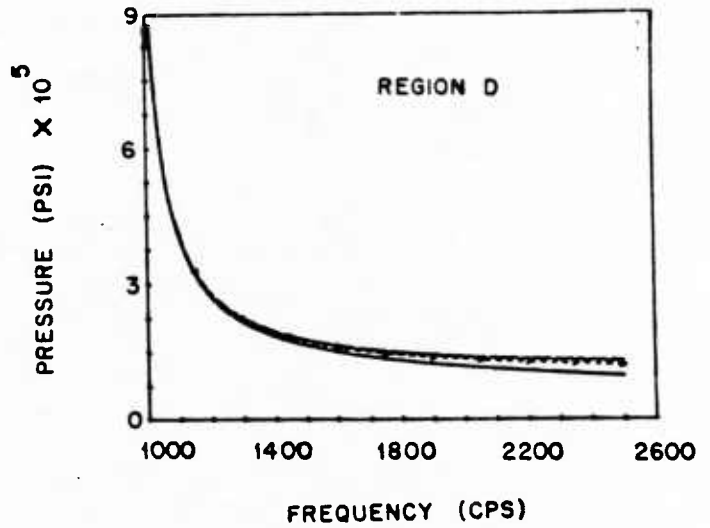
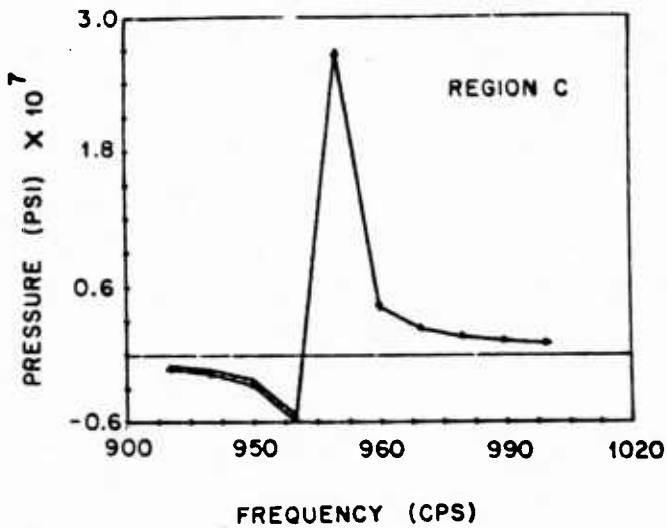
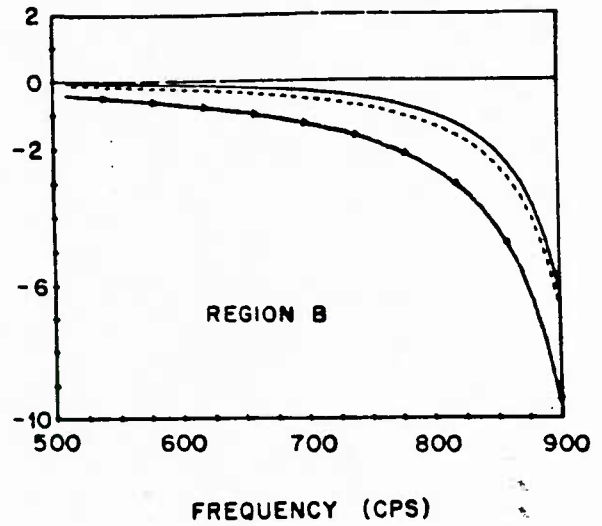
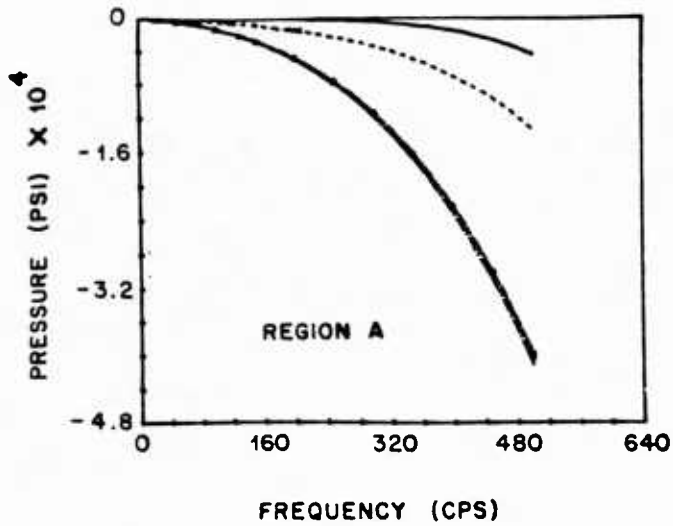


FIG. 26 COMPARISON OF PRESSURES OBTAINED FROM EXACT AND APPROXIMATE SOLUTIONS (n = 0 , m = 8)

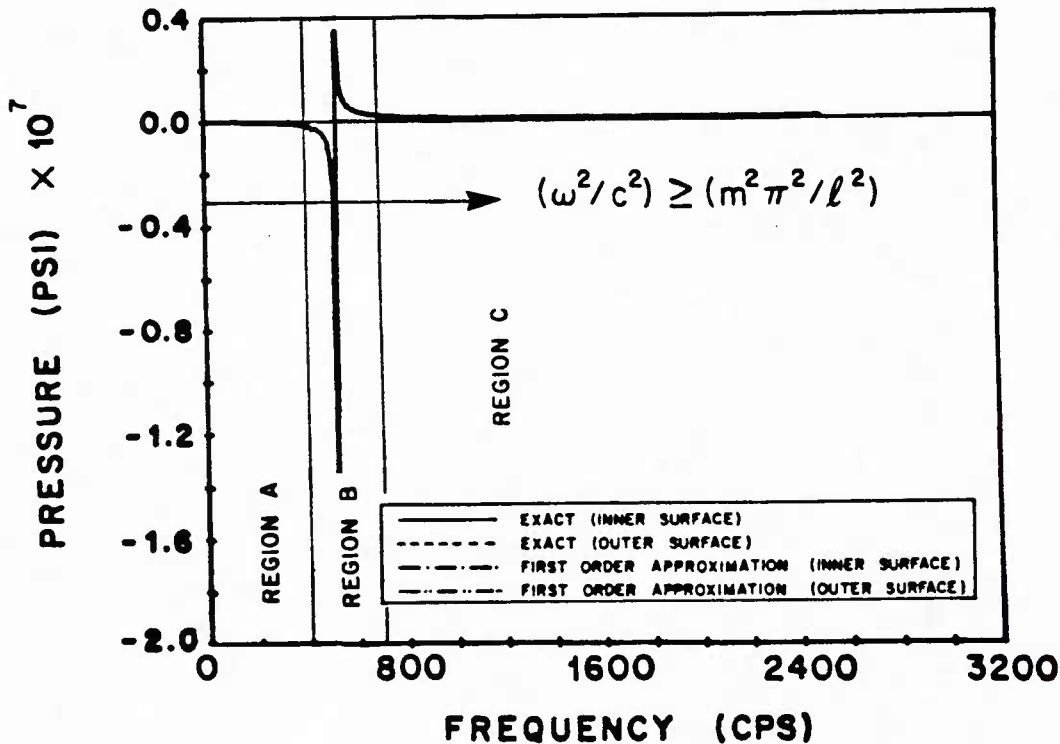
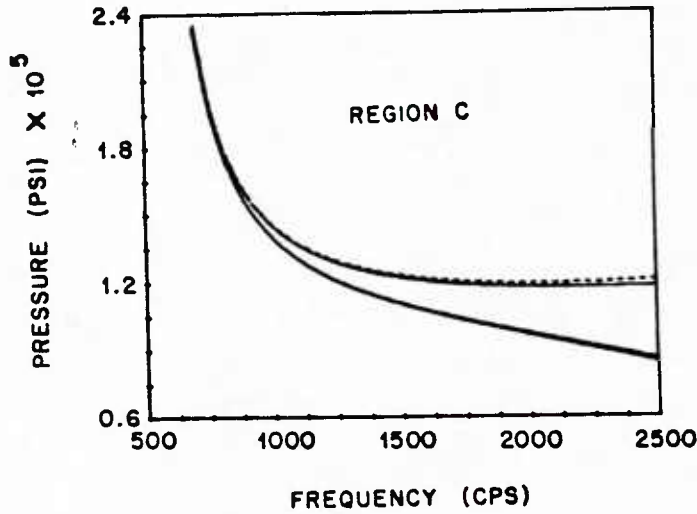
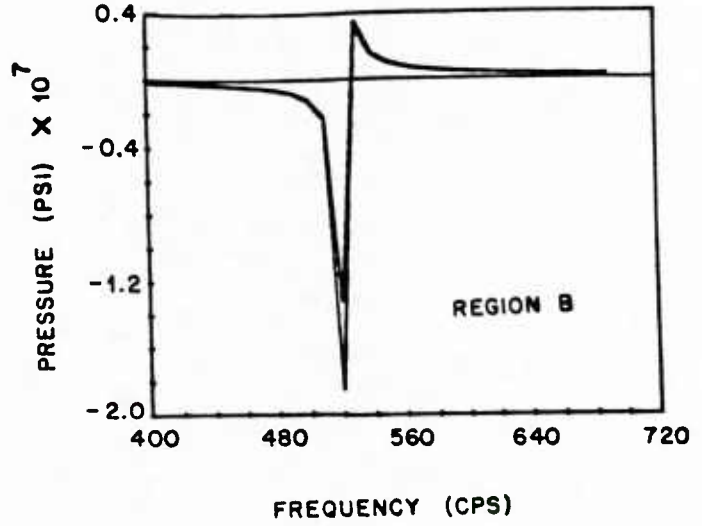
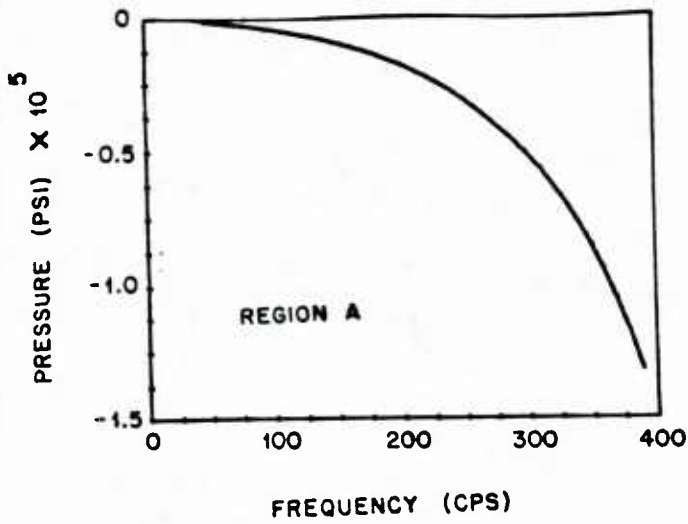


FIG. 27 COMPARISON OF PRESSURES OBTAINED FROM EXACT AND APPROXIMATE SOLUTIONS ($n = 1, m = 0$)

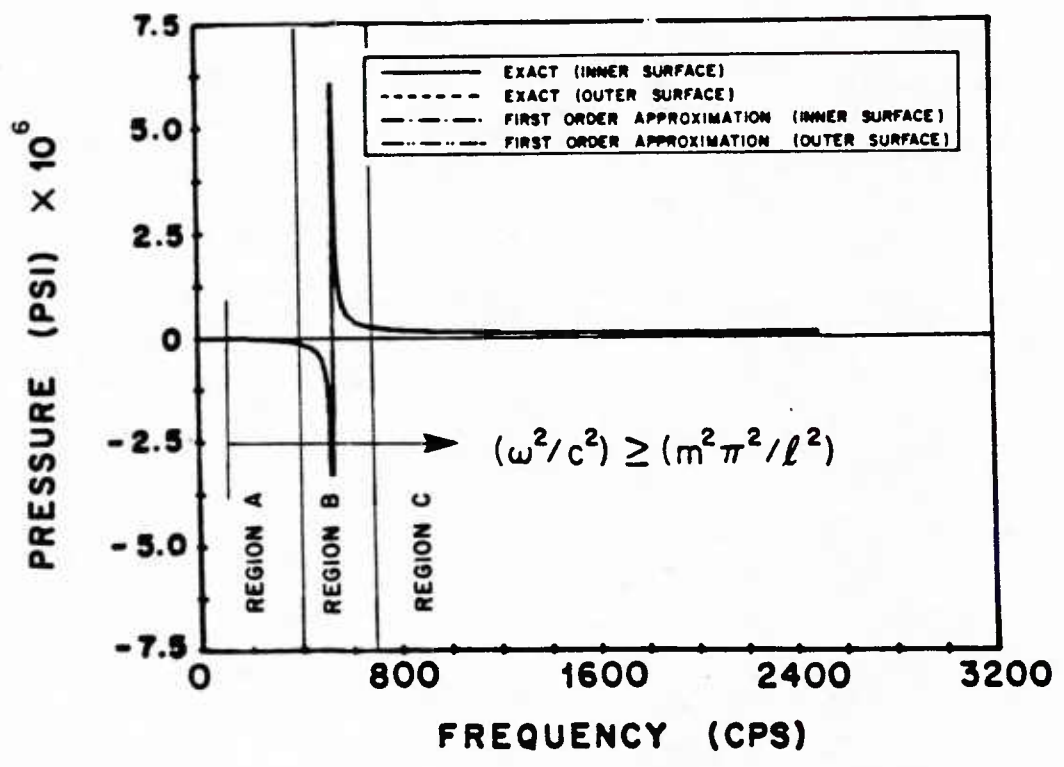
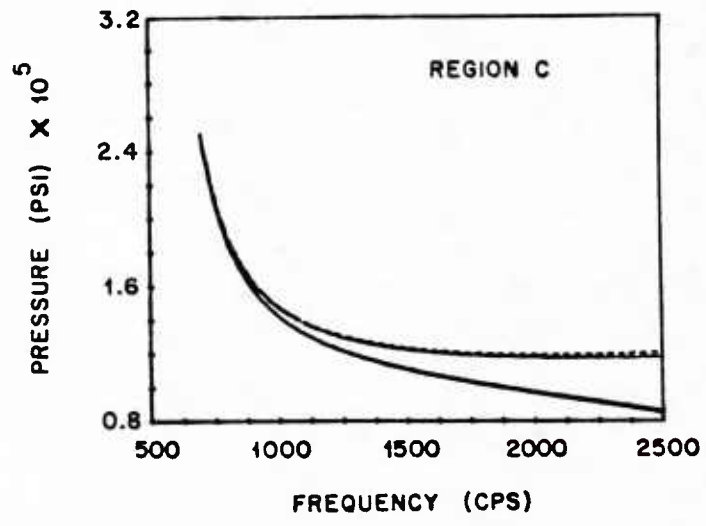
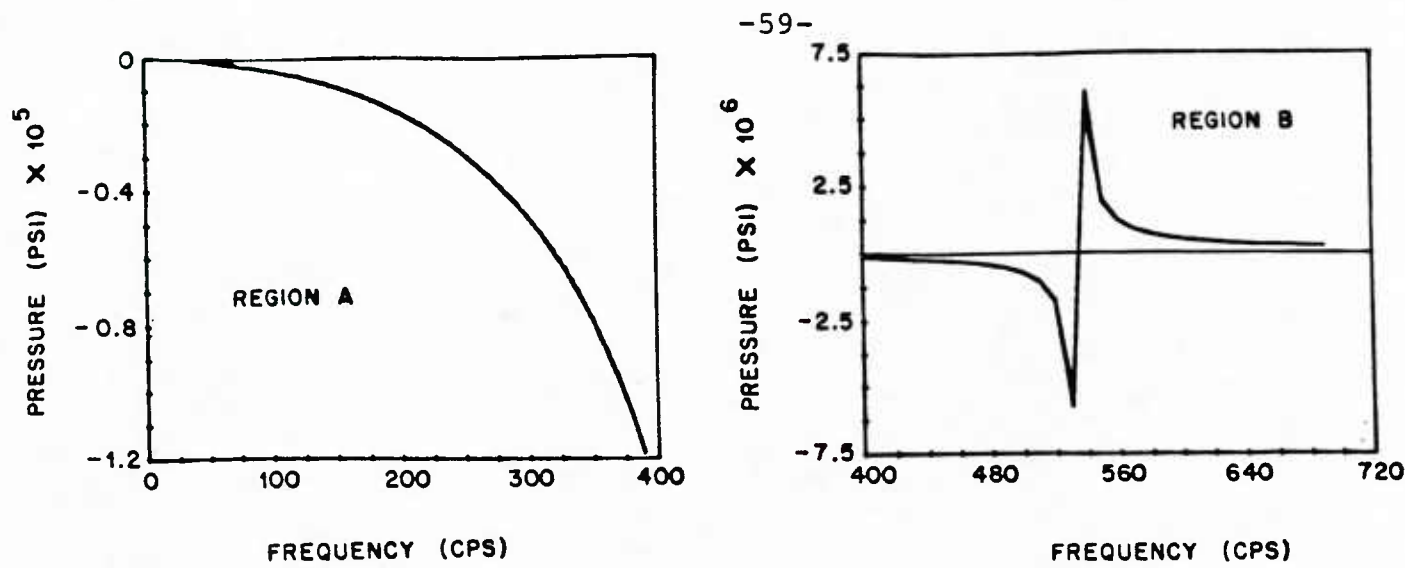


FIG. 28 COMPARISON OF PRESSURES OBTAINED FROM EXACT AND APPROXIMATE SOLUTIONS ($n = 1, m = 1$)

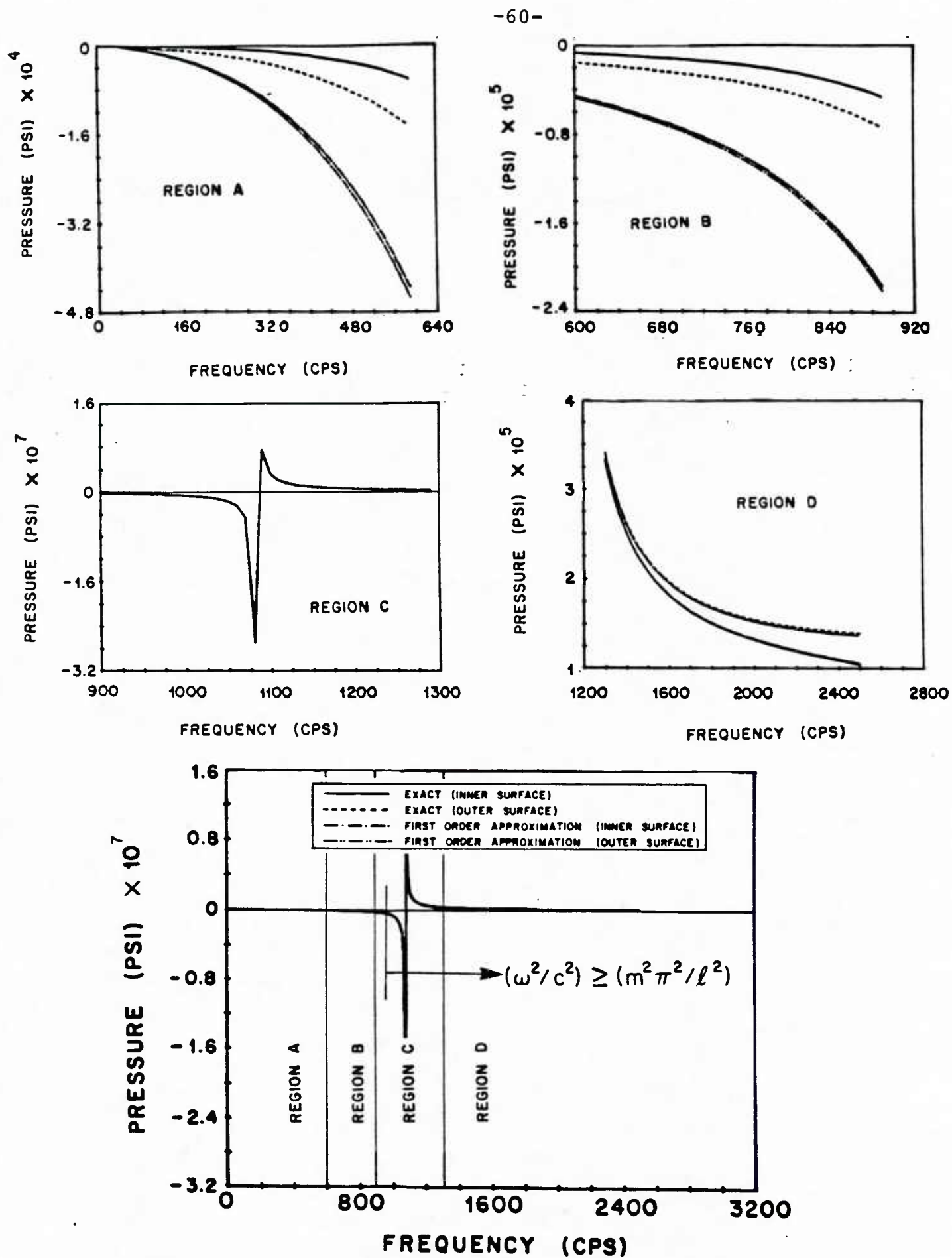


FIG. 29 COMPARISON OF PRESSURES OBTAINED FROM EXACT AND APPROXIMATE SOLUTIONS (n = 1 , m = 8)

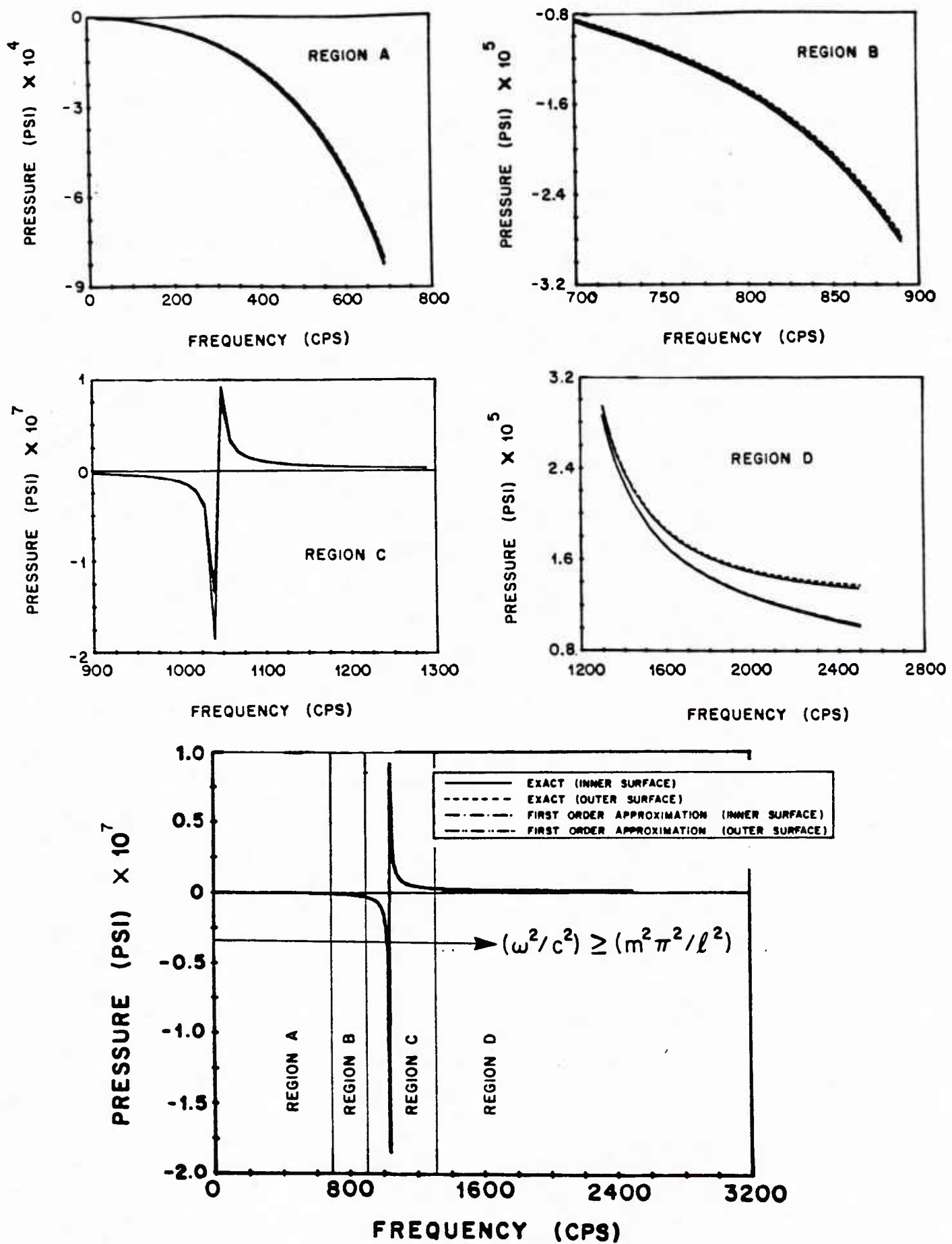


FIG. 30 COMPARISON OF PRESSURES OBTAINED FROM EXACT AND APPROXIMATE SOLUTIONS (n=2 ,m=0)

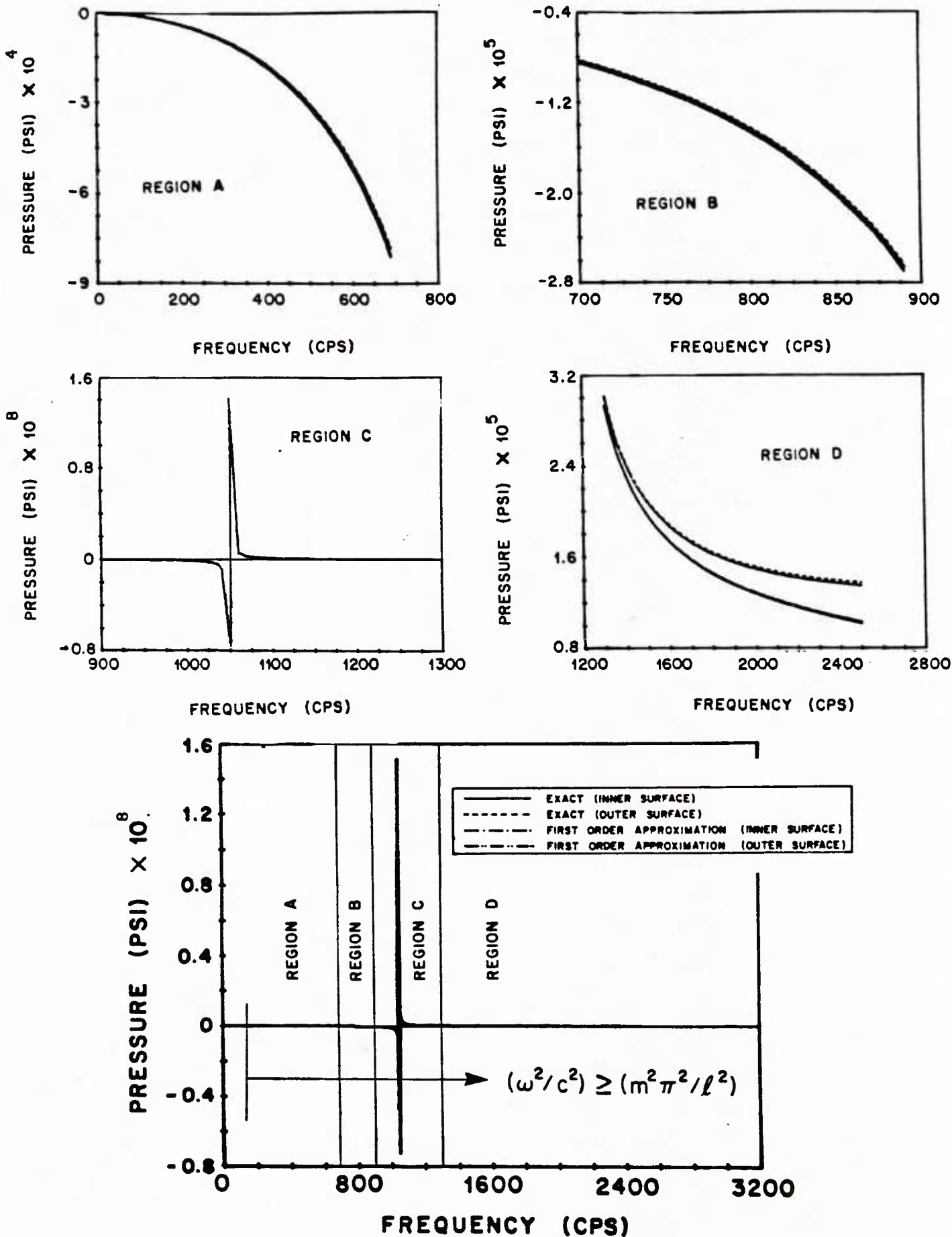


FIG. 31 COMPARISON OF PRESSURES OBTAINED FROM EXACT AND APPROXIMATE SOLUTIONS (n = 2 , m = 1)

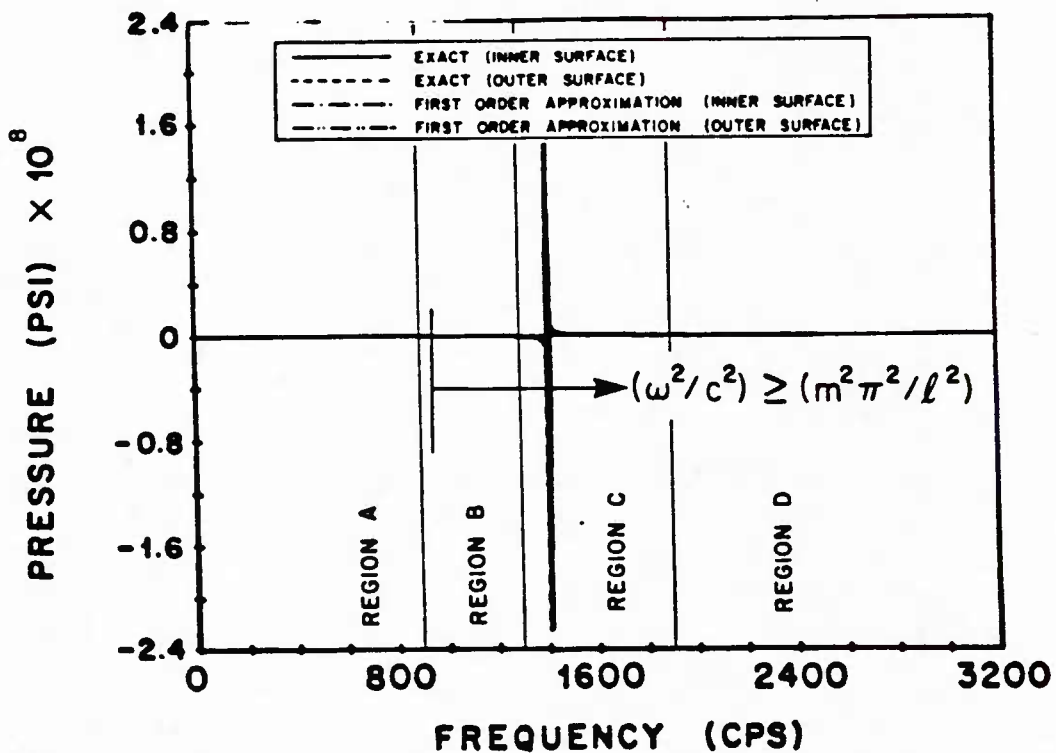
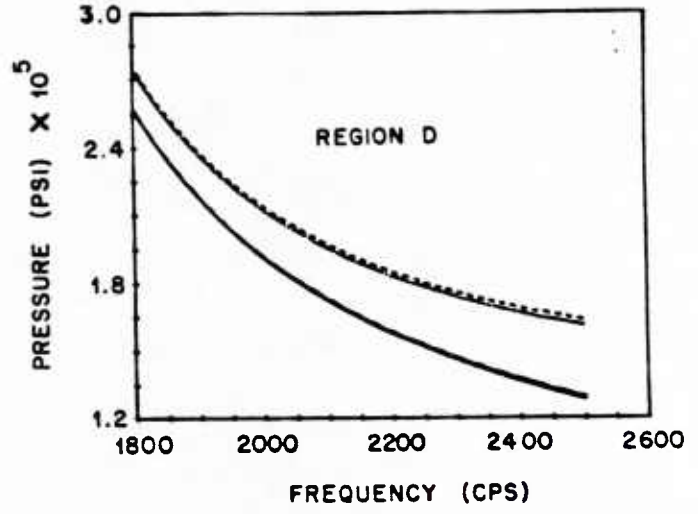
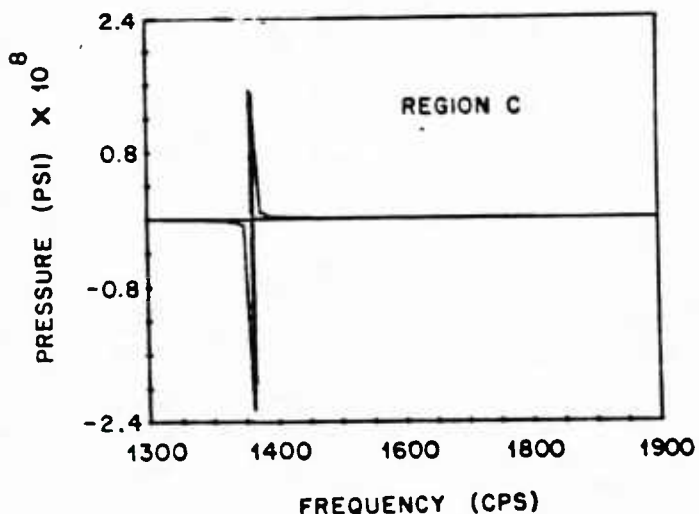
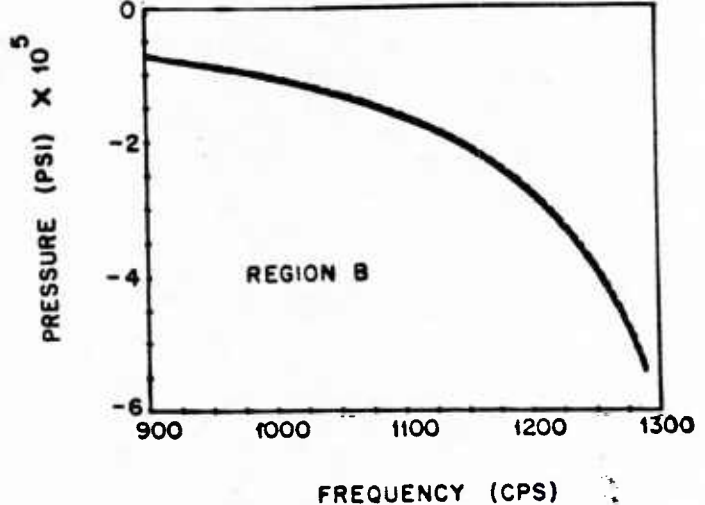
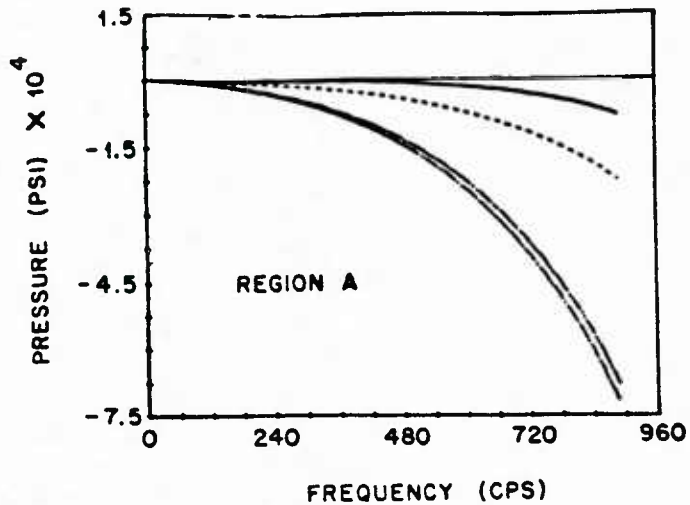


FIG. 32 COMPARISON OF PRESSURES OBTAINED FROM EXACT AND APPROXIMATE SOLUTIONS (n = 2 , m = 8)